Theses and Dissertations   1. Thesis and Dissertation Collection, all items

1992-12

Rapid marine cyclogenesis forecast sensitivity to high resolution sea surface temperatures during ERICA IOP-5

DeCaria, Marcia A.

Monterey, California. Naval Postgraduate School

http://hdl.handle.net/10945/23758

Unclassified
SECURITY CLASSIFICATION OF THIS PAGE

REPORT DOCUMENTATION PAGE

1a REPORT SECURITY CLASSIFICATION	1b RESTRICTIVE MARKINGS
Unclassified	

2a SECURITY CLASSIFICATION AUTHORITY	3 DISTRIBUTION / AVAILABILITY OF REPORT
	Approved for public release; distribution
2b DECLASSIFICATION / DOWNGRADING SCHEDULE	is unlimited

4 PERFORMING ORGANIZATION REPORT NUMBER(S)	5 MONITORING ORGANIZATION REPORT NUMBER(S)

6a NAME OF PERFORMING ORGANIZATION	6b OFFICE SYMBOL (If applicable)	7a NAME OF MONITORING ORGANIZATION
Naval Postgraduate School	35	Naval Postgraduate School

6c. ADDRESS (City, State, and ZIP Code)	7b ADDRESS (City, State and ZIP Code)
Monterey, CA 93943-5000	Monterey, CA 93943-5000

8a NAME OF FUNDING / SPONSORING ORGANIZATION	8b OFFICE SYMBOL (It applicable)	9 PROCUREMENT INSTRUMENT IDENTIFICATION NUMBER

8c. ADDRESS (City, State, and ZIP Code)	10 SOURCE OF FUNDING NUMBERS			
	PROGRAM ELEMENT NO	PROJECT NO	TASK NO	WORK UNIT ACCESSION NO

11 TITLE (Include Security Classification)
RAPID MARINE CYCLOGENESIS FORECAST SENSITIVITY
TO HIGH RESOLUTION SEA SURFACE TEMPERATURES DURING ERICA IOP-5

12 PERSONAL AUTHOR(S)
DeCaria, Marcia Ann

13a TYPE OF REPORT	13b TIME COVERED	14 DATE OF REPORT (Year, Month Day)	15 PAGE COUNT
Master's Thesis	FROM _____ TO _____	1992 December	91

16 SUPPLEMENTARY NOTATION
The views expressed in this thesis are those of the author and do not reflect the
official policy or position of the Department of Defense or the U.S. Government.

17	COSATI CODES		18 SUBJECT TERMS (Continue on reverse if necessary and identify by block number)
FIELD	GROUP	SUB-GROUP	SST resolution, ERICA, surface fluxes, rapid cyclogenesis

19 ABSTRACT (Continue on reverse if necessary and identify by block number)
The influence of high resolution sea surface temperatures (SST) on Nested Grid Model
(NGM) predictions of rapid marine cyclogenesis is examined. Satellite data provides a
gridded SST analysis with a resolution of 50 km. Forecasts using the operational
"blended" SST analysis with a neutral stratification assumed in the calculation of the
surface exchange coefficient over the ocean are compared to forecasts using the high
resolution SST analysis with a stability dependent surface exchange coefficient.
Further comparison is made to NGM forecasts with no surface fluxes. This study covers
the Intensive Observation Period (IOP) 5 of the Experiment on Rapidly Intensifying
Cyclones over the Atlantic (ERICA). Results show little sensitivity of central
pressure and storm position to the high resolution SST's. However, differences in
mesoscale features are present, primarily surface fluxes, precipitation, and frontal
circulations.

20 DISTRIBUTION / AVAILABILITY OF ABSTRACT	21 ABSTRACT SECURITY CLASSIFICATION
☒ UNCLASSIFIED/UNLIMITED ☐ SAME AS RPT ☐ DTIC USERS	Unclassified
22a NAME OF RESPONSIBLE INDIVIDUAL	22b TELEPHONE (Include Area Code)	22c OFFICE SYMBOL
Patricia M. Pauley	408-656-3275	63PA

DD Form 1473, JUN 86   Previous editions are obsolete   SECURITY CLASSIFICATION OF THIS PAGE

S/N 0102-LF-014-6603

Unclassified

T260075

i

Rapid Marine Cyclogenesis Forecast Sensitivity
to High Resolution Sea Surface Temperatures
during ERICA IOP-5

by

Marcia A. DeCaria
Lieutenant, United States Navy
B.A., University of Montana

Submitted in partial fulfillment
of the requirements for the degree of

MASTER OF SCIENCE IN METEOROLOGY AND PHYSICAL
OCEANOGRAPHY

from the

NAVAL POSTGRADUATE SCHOOL
December 1992

ABSTRACT

The influence of high resolution sea surface temperatures (SST) on Nested Grid Model (NGM) predictions of rapid marine cyclogenesis is examined. Satellite data provides a gridded SST analysis with a resolution of 50 km. Forecasts using the operational "blended" SST analysis with a neutral stratification assumed in the calculation of surface exchange coefficient over the ocean are compared to forecasts using the high resolution SST analysis with a stability dependent surface exchange coefficient. Further comparison is made to NGM forecasts with no surface fluxes. This study covers the Intensive Observation Period (IOP) 5 of the Experiment on Rapidly Intensifying Cyclones over the Atlantic (ERICA). Results show little sensitivity of central pressure and storm position to the high resolution SST's. However, differences in mesoscale features are present, primarily surface fluxes, precipitation, and frontal circulations.

TABLE OF CONTENTS

LIST OF FIGURES

ACKNOWLEDGEMENTS

I wish to thank Dr. Pat Pauley for her never-ending support and enthusiasm for this project. It could not have been completed without her extra patience and guidance, which included completing an NPS thesis long distance. My thanks also to Dr. Wendell Nuss, who sparked my interest in studying storm behavior along the Gulf Stream and helped me learn about GENAL and the IDEA Lab. This project would not have been completed so quickly without the challenge provided by my curricular officer, CDR Tim Cummings. A final recognition goes to the NPS Meteorology Department, a group of total professionals who always go out of their way to help the students.

On a more personal note, Alex, thank you for your encouragement. Your support throughout this entire evolution has been invaluable.

I. INTRODUCTION

The exact role of both sensible and latent heat fluxes in rapid cyclogenesis over the ocean is still in question. Petterssen et al. (1962) concluded initial development was mainly due to thermal advections in the lower troposphere. However, including both sensible and latent heat fluxes in thickness tendency calculations (1000 to 500 mb) led to improvement in all ten cases studied. They examined several different developmental stages of storms, and compared the 3-hr thickness change with adiabatic effects only to the 3-hr thickness change with surface fluxes added. They separated the vertical p-velocity (omega) into two parts ($\omega \equiv \omega_A + \omega_B$); ω_A corresponds to dry adiabatic processes and ω_B is the additional motion due to the supply of sensible heat and the release of latent heat. The addition of the surface fluxes showed a more realistic depiction as verified by the observed analysis.

More recently, Davis and Emanuel (1988) tested the hypothesis that routinely underpredicted intensities of rapidly deepening cyclones by the LFM were due to an inadequate representation of surface fluxes from the sea surface. For the more rapid deepeners in their study, a strong correlation was found between the underprediction of the deepening rate and the magnitude of potential warming due to sensible and latent heat fluxes. Thus, they concluded that the underlying ocean's in-situ effects may be crucial for rapid development.

On the other hand, Kuo and Low-Nam (1990) concluded that surface fluxes had virtually no impact on forecasting cyclone development by the PSU/NCAR mesoscale model for 24 h forecasts. This study provided a fairly comprehensive view of numerical model behavior through its variety of experiments performed on nine cases of rapid oceanic cyclogenesis in the Atlantic. In 1991, Kuo and colleagues published new findings which modified the conclusions of Kuo's own paper published the year prior. Kuo et al. (1991) discovered that by initializing the PSU/NCAR model earlier, during the early development stage instead of during the rapid development stage, surface energy fluxes affected a cyclone up through the rapid development stage. When initialized 24 hours prior to the period of most rapid deepening, results of the addition of fluxes into the model physics were: deeper low central pressure values, coastal frontogenesis depiction, formation of a shallow frontal circulation, reduced static stability in and near the frontal region, and enhanced precipitation. Their results agreed with those of Reed and Simmons (1991) stating that surface fluxes had little impact on further cyclone development once the rapid deepening phase had begun. These studies suggest that the importance of surface fluxes is primarily in "preconditioning" the environment prior to initial cyclogenesis.

The question of the exact role of surface fluxes is further complicated by the dependence of surface fluxes on sea surface temperature (SST) distribution in numerical weather prediction models. Ballentine (1980) showed that over regions with a large SST gradient, storms tend to intensify and follow a path parallel to the isotherms. This behavior was seen in many of the storms observed in the Experiment on Rapidly

2

Intensifying Cyclones over the Atlantic (ERICA; Kreitzberg, personal communication). A sensitivity study by Mailhot and Chouinard (1989) with the RFE meso-alpha scale model compared forecasts based on three different SST distributions. Their experiment compared two resolutions of SST distribution (100 and 190 km resolution) based on the Scripps climatology to the enhanced NOAA NESDIS 1° resolution monthly averaged SST's. They found that the impact of the higher resolution SST's was mainly in lower levels. The enhanced SST analysis had a better position and central pressure value of the offshore surface low, and the atmospheric thermal gradient had a more pronounced S shape. Vertical representation of the warm front showed that the enhanced SST analysis forecast produced a more intense frontal zone characterized by steeper isentropes, deeper vertical circulations and larger moisture gradients. They concluded that the formation and maintenance of an intense southerly low level jet (LLJ) ahead of the surface cold front appears to be instrumental throughout the rapid deepening phase.

Warner et al. (1990) had similar results when they compared 12 h forecasts after initialization with a high and low resolution SST distribution. They compared NOAA's 14 km resolution SST to the Navy's smoother operational SST analysis from Fleet Numerical Oceanography Center (FNOC) with 381 km resolution. When these two SST fields were input into the PSU/NCAR mesoscale model they found that similar dynamic marine atmospheric boundary layer (MABL) responses occurred; however, larger-scale structural features were weaker and smaller-scale ones were frequently absent with the FNOC SST. The higher resolution NOAA SST produced results which compared better with the observations: the MABL

3

front across the Gulf Stream was four times stronger; the surface pressure gradient was three times larger; and precipitation amounts were double.

Lapenta et al. (1992) employed a different technique for their SST sensitivity study. They used the same SST analysis for the Gulf Stream region for the three experiments using the Drexel LAMPS model, but displaced it 350 km north and south from the control experiment to observe the effect of the SST front placement on ERICA IOP-4. They found that the north and control experiments produced similar results, while the south was quite different. The south experiment had the storm track north of the Gulf Stream front, over colder water. Thus, it was not preconditioned by the heating and moistening of the MABL while both the control and north experiments were fully preconditioned. As a result, the south experiment showed a decreased intensification rate, lowered precipitation, and weaker central pressure. The storm tracks of all three experiments were interestingly similar, with the track only being displaced 50 km when the SST front was displaced 350 km. Lapenta et al. (1992) also addressed the problem of specifying initial conditions of the large-scale flow to ensure reasonable initial adjustment to the SST field. If the initial MABL structure and SST field are significantly out of balance, the resulting fluxes may be unrealistically high. They used a "nudging term" to lessen that effect.

The present research seeks to expand on these earlier results by examining sensitivity to SST distribution for an operational model, the National Meteorological Center's (NMC) Nested Grid Model (NGM). The operational NGM uses the rather smooth "blended" SST analysis. The operational forecast for the ERICA Intensive Operating Period (IOP) 5

storm will be contrasted with ones using a higher resolution satellite-derived SST analysis and one with no surface fluxes. These forecasts were all initialized 24 h prior to the beginning of rapid cyclogenesis to allow the surface fluxes to precondition the MABL, as suggested by the Kuo and Low-Nam (1990) and Kuo et al. (1991) results. Although this research does not directly address the question of the pre-conditioning vs. in-situ effects of surface fluxes, it will examine sensitivity to SST distribution with this question in mind.

II. BACKGROUND

Meteorologists have been intensively exploring the dynamics of rapid marine cyclogenesis for the past decade. Sanders and Gyakum (1980) first defined the "bomb" and its climatology, which spawned further investigation into causes of these dangerous storms. Their definition of a rapid cyclogenesis event is an extratropical cyclone whose central sea level pressure decreases at least 1 mb/h for 24h, normalized by $\sin \phi$ / $\sin 60°$, where ϕ is the latitude of interest. The resulting critical rate, defined as 1 Bergeron, is 19 mb / 24 hr at 45°N.

The east coast of the United States is one of the regions where rapid cyclogenesis is favored (Sanders and Gyakum 1980, Roebber 1984). This is largely due to climatological baroclinic conditions which are caused by winter continental cold air outbreaks overlying the warm waters of the Gulf Stream. Since this is a region where commercial and military shipping is heavy, intensive experiments have been funded to explore the mechanics of their development and thus better predict these potentially destructive storms.

The latest field experiment on rapid cyclogenesis in the Gulf Stream region was the ONR-sponsored Experiment on Rapidly Intensifying Cyclones over the Atlantic (ERICA). ERICA scientists have been studying the physical mechanisms and processes, and their critical spatial and temporal combinations causing rapid marine cyclogenesis, since the field phase which took place from December 1988 to February 1989 (Hadlock and Kreitzberg 1988). The objectives of the program were to:

6

1. understand the fundamental physical processes occurring in the
      atmosphere during rapid intensification of cyclones at sea,

   2. determine those physical processes that need to be incorporated
      into dynamical prediction models through efficient
      parameterizations if necessary, and

   3. identify measurable precursors that must be incorporated into
      the initial analysis for accurate and detailed operational model
      predictions.

Several secondary questions were posed for the ERICA study, one of which

is the role of sea surface temperature distribution in the numerical

prediction of rapid cyclogenesis. It is this aspect of rapid cyclogenesis

that the present research focuses on.

   Figure 1, from Hadlock and Kreitzberg (1988), shows an idealized

structure of features that could interact during the rapid intensification

phase. The diagram includes an upper-level trough located to the west of

an upper-level jet. It also shows a considerable vertical tilt to the

system, with the surface cold front located parallel to and east of the

upper-level trough. The jet is positioned such that the associated upper-

level divergence is located to the northeast of the surface low. Upper-

level divergence ahead of the storm is required for rapid intensification.

The low-level jet enhances heat and moisture advections from the south

into the region near the low center, which serve to enhance both sensible

and latent heating of the atmosphere.

   Divergence is a prominent feature at upper levels, contributing to a

net reduction of mass in the air column, and thus a mechanism for surface

pressure falls in the presence of low-level convergence. Divergence aloft

is approximated by positive vorticity advection (PVA) in the 500 mb

trough/ridge pattern. Ageostrophic effects in the left exit region and/or

right entrance region of upper-level jet streaks add to divergence aloft (Uccellini 1990).

Another relevant upper-level process is tropopause folding, with subsidence in the upper and middle troposphere contributing to upper-level frontogenesis and bringing cold, dry stratospheric air down to the 500 to 700 mb layer. Uccellini (1990) discussed several studies which point to a causal relationship between tropopause folding with the accompanying extrusion of stratospheric air and the subsequent evolution of a surface cyclone. By the principle of conservation of isentropic potential vorticity (IPV), where IPV $= -(\zeta_\theta + f)\partial\theta/\partial p$, static stability $(-\partial\theta/\partial p)$ decreases significantly as stratospheric air descends into the troposphere. Therefore, absolute vorticity increases as long as the stratospheric values of IPV are preserved. This folding is more likely to occur when the jet streak and upper-level trough occur as shown in Fig. 1.

Low-level processes that likely affect the deepening rates of cyclogenesis over the ocean include: thermal advection, sensible and latent heat fluxes, and latent heating.

Extratropical cyclogenesis is marked by a baroclinic zone near the surface that evolves into an "S"-shaped thermal pattern during the period of most rapid intensification. Sharp thermal gradients are commonly found in the vicinity of the Gulf Stream in winter, created by the collision of warm, moist air originating over the warm waters of the Gulf Stream with cold, dry continental air flowing seaward. Uccellini (1990) stated that a low-level jet (LLJ) which crosses this oceanic thermal gradient at a significant angle yields a higher Laplacian of the thermal advection, such that there will be cold and warm air advection to the west and east of the

8

storm center, respectively. Warm air advection forces ascent and low-level convergence with cyclonic development, as per the Petterssen Development Equation. Differential thermal advections amplify the upper level wave, which increases upper level vorticity, which causes greater positive vorticity advection aloft, and so on, continuing to intensify the storm until it is vertically stacked.

Sensible heating of the atmosphere over the Gulf Stream water reduces the static stability during and just prior to rapid cyclogenesis. As can be seen using the omega equation, reducing static stability reduces its braking of upward motion, thereby enhancing conditions favorable to rapid cyclogenesis (Wash, et al. 1988). The vertical gradient of omega ($\partial\omega/\partial p$) is equal to convergence ($-\nabla\cdot V$) at a particular level. By the vorticity equation, convergence contributes to spin-up ($\partial\zeta/\partial t > 0$).

The feedback mechanism between dynamical and diabatic processes results in an increased deepening rate of the surface low. Sensible and latent heat fluxes increase low-level thermal and moisture gradients, increasing baroclinicity. The enhanced baroclinicity increases thermal advection; at lower levels, warm air advection increases the propagation rate.

The latent heat flux (later referred to as moisture flux) moistens the boundary layer and provides for enhanced latent heating. Baker (1991) determined that latent heating during ERICA IOP-5 had a significant impact on the intensity of the storm. Withholding latent heat release from the NGM significantly decreased the intensity of not only the surface cyclone, but its associated 500 mb trough/ridge system as well. Since latent

heating played such an important role during this storm, the moisture fluxes and the vertical velocity will be examined in subsequent chapters.

III. MODEL DESCRIPTION

This study examines the sensitivity of NGM forecasts of a rapidly deepening oceanic extratropical cyclone to the specification of the sea surface temperature (SST) field. Three different experiments, referred to as OPNL, HSST, and NSF, respectively, are examined and compared:

1. The NGM forecast with the operational "blended" SST analysis (OPNL).

2. The NGM forecast with a higher resolution satellite-derived SST analysis, utilizing a stability-dependent surface exchange coefficient over water as well as over land (HSST).

3. The NGM forecast without surface fluxes (NSF).

All three experiments were initialized at 1200 UTC 18 January 1989 from the operational data stream. Initialization occurred 48 h prior to the minimum central pressure of IOP-5, 24 h prior to rapid cyclogenesis.

The operational NGM (see Appendix B for a more complete model description) uses the NMC global blended SST analysis with a grid spacing of 2° (Rao 1989). This analysis utilizes all in-situ data from ships and fixed buoys, as well as satellite data collected during the previous 15 days. The in-situ data and satellite data are independently averaged in 2° x 2° boxes. Temperatures in boxes with insufficient data are obtained through extrapolation of anomaly fields to preserve the mean features of the global distribution. A nonlinear filter is applied to each of the data fields to produce separate in-situ and satellite analyses. The final SST product is then obtained by blending the satellite-derived SST

11

analysis with the in-situ analysis. Regions with five or more in-situ SST observations utilize the data as internal boundary values. The Laplacian of the satellite analysis (based on 10 or more satellite observations) is used as a forcing function to preserve the shape of the field ($\nabla^2 = 0$ if there are less than 10 observations). The blended analysis is considered an improvement over the fields obtained from either the in-situ data or the satellite data alone (Feit 1986). This analysis serves as the skin temperature for the longwave radiation, sensible heat fluxes, and latent heat fluxes over water in the NGM (Hoke et al. 1989).

Figure 2a shows the global blended SST analysis used in the OPNL experiment. The NGM C-grid was rotated 20 degrees to the east of the operational configuration for all three experiments to ensure complete coverage of the IOP-5 storm area and to minimize boundary effects. A 50 x 70 output domain was used to maximize vertical and horizontal resolution within the constraints imposed by limited disk storage at NMC.

The high resolution experiment (HSST) made use of the NOAA/NESS Multi-Channel Sea Surface Temperature (MCSST) with a grid spacing of $0.5°$ lat x $0.5°$ lon (Fig. 2b). The MCSST analysis uses only satellite data from the Advanced Very High Resolution Radiometer (AVHRR) aboard NOAA's TIROS polar orbiting satellites (Rao 1989). Data is collected from four channels: two thermal infrared (IR), one near IR, and one visible. Approximately 75,000 daytime and 25,000 nighttime SST observations are collected daily, at a resolution of 4 km. The observations are then box-averaged to 8 km and objectively analyzed using inverse distance squared weighting to provide gridded SST fields from which contoured charts are produced. A cloud filtering technique is performed on the satellite data as described

by McClain et al. (1985). Combinations of AVHRR channels are used to detect the presence of clouds in small arrays of data. Only cloud-free data are processed for MCSST's. The HSST experiment checked that the data point was within the MCSST domain (5°N - 53°N, 100°W - 52°W) and that the temperature was above freezing. Then a bilinear interpolation to the NGM polar-stereographic C-grid was performed. Outside the domain of the MCSST analysis, the blended analysis as described above was used. No attempt was made to smooth the boundaries between these two analyses since no abrupt discontinuities were apparent (although the boundary itself is apparent in Fig. 2b at 52°W).

A stability-dependent surface exchange coefficient over water was also used in the HSST experiment. This modification was subsequently implemented in the NGM, effective 7 November 1990 (Petersen, et al. 1991). Prior to that date, the operational NGM a used stability-dependent exchange coefficient in the calculation of surface drag, evaporation and sensible heat flux only over land. Over water, neutral stability was assumed, resulting in the misrepresentation of surface fluxes when stability deviated significantly from neutral. This new surface flux parameterization produces more realistic evaporation rates, and has shown increased evaporation into cold air masses over the Gulf Stream.

All surface fluxes were turned off during the forecast period for the NSF experiment. Any sensitivity to the resolution of the SST analysis is expected to be smaller than the sensitivity to surface fluxes themselves. Comparisons with the NSF forecast serve to place the differences between OPNL and HSST experiments in context.

13

IV. SYNOPTIC DISCUSSION

This section will first examine the development of the ERICA IOP-5 storm using the NGM analyses as "ground truth". Baker (1991) examined both NGM analyses and Sanders' manual analyses for IOP-5, and determined that differences between them were negligible. Next, the three experimental forecasts (OPNL, HSST, and NSF) initialized at 1200 UTC 18 January 1989 will be compared to each other and to the NGM analyses to determine forecast accuracy. These forecasts were initialized 24 hours prior to rapid cyclogenesis, allowing pre-conditioning of the maritime boundary layer by surface fluxes as described by Kuo et al. (1991).

Cyclogenesis for IOP-5 was evident at about 1200 UTC 19 January 1989 (12Z/19). Within 24 hours, the surface central pressure dropped from 1005 mb to 970 mb (35 mb / 24 hr), qualifying the storm as a rapid deepener. By about 1200 UTC 20 Jan 1989 (12Z/20), the storm reached maximum intensity, with winds in excess of 40 kts near the storm center. The storm was vertically stacked at that time and began to fill.

A. DISCUSSION OF NGM ANALYSES

1. 1200 UTC 18 January Analysis

At initialization, 24 h prior to surface development, a 1005 mb low was centered near Green Bay, Wisconsin (Fig. 3a). The surface low which later became the IOP-5 storm had not yet appeared, although there was a 1021 mb low pressure center off the coast of Georgia. This low moved northward and deepened to 1016 mb in the next 12 h, and appears to

14

be the incipient IOP-5 low. Figure 3b shows a moderately strong absolute vorticity maximum (18×10^{-5} s^{-1}) at 500 mb in the base of a trough which extended from Minnesota through Iowa and Missouri to Kansas.

2. 1200 UTC 19 January Analysis

The incipient IOP-5 low was well depicted by the NGM analysis (Fig. 4a) by 12Z/19. It had developed a closed low center at 38N, 68W off Cape Hatteras and deepened to 1005 mb. The thickness distribution in the vicinity of the low showed an s-shaped pattern, indicating warm and cold air advection and the beginnings of baroclinic wave amplification.

At upper levels, the 500 mb shortwave had moved very quickly to the east (Fig. 4b) and amplified. A strong vorticity maximum of 26×10^{-5} s^{-1} was located about 4° west of the surface low, producing significant PVA aloft over the surface cyclone. This was a primary forcing mechanism for storm intensification during the next 12 hours.

3. 0000 UTC 20 January Analysis

By 00Z/20, the storm deepened 20 mb to a central pressure of 985 mb and moved extremely rapidly to a position of 41N, 57W, a speed of about 40 kts (Fig.5a). Thickness contours showed a more definite s-shape near the storm and therefore stronger thermal advection at lower levels.

At 500 mb, the shortwave position was still to the south and west of the surface low, which provided continued upper-level forcing for the storm system (Fig.5b). The analyzed vorticity maximum had decreased slightly to 24×10^{-5} s^{-1}, with the 500 mb trough parallel and west of the surface cold front. PVA was still evident over the storm center, suggesting further intensification.

15

4.   1200 UTC 20 January Analysis

By 12Z/20, the storm was vertically stacked, indicating that it had reached its maximum intensity (Figs. 6a and 6b). The central pressure of the surface low had deepened to 970 mb by this time. The storm's movement had slowed from the previous 12 hours, placing the low center at 44N, 50W. The s-shaped pattern of the thickness contours indicates continuation of significant thermal advections at lower levels which helped to build the closed low aloft.

At 500 mb, the NGM analyzed a high amplitude shortwave trough with a closed low centered over the surface low. The vorticity maximum of 26×10^{-5} s^{-1} was located south and east of the surface low, a position unfavorable for future intensification at the surface.

B.   MODEL COMPARISON AND FORECAST VERIFICATION

Examining the three experimental NGM forecasts and comparing them to the NGM analyses reveals a pattern of errors for the forecasts initialized at 12Z/18. Overall, the surface forecasts were weak in deepening the storm and slow to move it northeastward. Figure 7 shows the storm tracks for the analyses and forecasts, while central pressures are summarized in Table 1. The 12Z/19 forecasted pressures and positions are taken from the triple point locations, which were derived by frontal placement based on vertical velocity, equivalent potential temperature, and relative humidity distributions at 950 mb.

16

TABLE 1

CENTRAL PRESSURE VALUES FOR NGM ANALYSES AND EXPERIMENTAL FORECASTS

Forecast time	Analysis	OPNL	HSST	NSF
12Z/19	1005	1010 (TP)	1010 (TP)	1010 (TP)
00Z/20	985	994	994	996
12Z/20	970	988	988	991

The following sections provide forecast verification for the three experiments and examine the differences between the three experiments regarding central pressure and position forecasts.

1.   **24 h Forecasts (VT 1200 UTC 19 Jan, hereafter, 12Z/19 Jan)**

At the beginning of the intensification period, none of the three 24 h forecasts (Fig. 8) showed a closed low out over the Atlantic, while the verifying analysis clearly showed one with a central pressure of 1005 mb. Instead, all three showed a trough in the region of the analyzed low, extending from a low over New York which is predicted to be 2 mb deeper and slightly south of its analyzed position. Frontal depictions on the forecast charts show a triple point located 2° east or northeast of the analyzed low suggesting the placement for the incipient IOP-5 storm. The s-shaped pattern of the thickness contours was also not as pronounced as in the analysis.

At 500 mb, all three forecasts showed a vorticity maximum of 18×10^{-5} s^{-1}, significantly weaker and located west of the analyzed maximum

of 26×10^{-5} s^{-1} (Fig.9). The OPNL, HSST, and NSF fields were almost identical in their vorticity and height distributions.

2. 36 h Forecasts (VT 00Z/20 Jan)

By the time of the 36 h forecast (Fig. 10) all three experiments portrayed the development of a closed low at the surface. All three were weak in forecasting the central pressure, with the OPNL and HSST being better than the NSF, even though 11 mb weaker than the NGM analysis. The three experiments were similar in their thickness distributions, with almost identical s-shaped patterns but with a thickness gradient that was not as great as in the NGM analysis. The HSST model moved the storm slightly faster than the OPNL model; both the HSST and OPNL moved the storm faster than NSF.

At 500 mb the NGM analysis showed a much deeper trough and stronger vorticity max than any of the three forecasts (Fig. 11). The predicted shortwave lagged behind the analyzed wave with a northeast-southwest orientation compared to the analyzed shortwave running north-south. All three experiments show a vorticity maximum of 20×10^{-5} s^{-1} compared to the analyzed value of 24×10^{-5} s^{-1}. There were differences also in the vorticity minimum in the downstream ridge, with a minimum value of 6×10^{-5} s^{-1} for the analysis and 8×10^{-5} s^{-1} for the three experiments.

3. 48 h Forecasts (VT 12Z/20)

The 48 h forecasts (Fig. 12) showed further deepening for the OPNL and HSST forecasts, from 992 mb to 988. These forecast pressures were 18 mb weaker than the actual central pressure, yielding about half the observed deepening rate for the storm. The NSF low deepened only to

18

991 mb. The thickness pattern of the OPNL and HSST had a less pronounced s-shaped pattern than seen at the 36 h forecast time. All three forecasts continued to be slow to move the storm, with the HSST having a slightly better position than the other two.

At 500 mb the HSST experiment strengthened the vorticity max to 26×10^{-5} s^{-1}, in agreement with the NGM analysis (Fig. 13). The OPNL and NSF experiments deepened the vorticity max to 24×10^{-5} s^{-1}. The positions of all three maxima, however, were about 7° to the west of the analyzed position. While the three experiments show an upper-level closed low, all three were weaker than the NGM analysis: the OPNL and HSST forecasts by 50m and the NSF forecast by 60m.

In summary, the three experimental forecasts were quite similar for the IOP-5 cyclogenetic event. They were all slow to deepen and move the cyclone as verified by the NGM analyses. The effect of turning off all surface fluxes was apparent in the later forecasts for the NSF experiment, as it failed to deepen the storm as much as OPNL and HSST at the lower levels after the 36 h forecast. A further look into differences between these forecasts is the topic of the next chapter of this paper.

V. RESULTS

The previous chapter examined synoptic-scale features as forecast by the three experiments and verified by the NGM analysis. This chapter focuses on boundary layer and mesoscale comparisons between the three experimental forecasts. Output in the form of NGM forecast fields was available for examination for the three experiments, with a vertical resolution of 50 mb and C-grid horizontal resolution. Difference fields were used to aid location of differences between experimental forecasts for the magnitude and distribution of particular parameters. Horizontal fields and cross sections will be used to show these differences.

A. HORIZONTAL FIELDS

1. Sensible Heat Flux

The first fields to be examined are the surface fluxes, since they yield the differences in input to the experimental forecasts for this storm that are most directly related to SST differences. The field which showed the largest difference between the OPNL and HSST experiments was the sensible heat flux, resulting from warmer water located farther north in the HSST experiment combined with the cold northerly winds. (Note that surface fluxes are zero by definition in the NSF experiment.) For the 24 h forecast, the flux maxima were located off the U.S. coast, in the region of surface cold air advection where air-sea temperature differences were the greatest and surface wind speeds were relatively large (Fig. 14). Maxima were 120 and 160 W m^{-2} for OPNL and HSST, respectively. The

20

difference in location of the maxima, however, led to flux differences up to 100 W m^{-2} near 37°N, 71°W. It apparent that the stronger flux for the HSST experiment is due to the stronger SST gradient in the vicinity of 38N, 72W (see Fig 2). As a result, the HSST experiment had warmer waters farther north than OPNL, increasing the air-sea temperature differences for HSST, thus causing higher sensible heat fluxes (and moisture fluxes, as described in the next section). In the vicinity of the warm front, HSST shows a surface heat flux which is as much as 40 W m^{-2} stronger than OPNL in spite of the relatively small values in the region.

By the 36 h forecast, the differences are even larger (Fig. 15). Maximum fluxes for OPNL and HSST in the cold sector are 90 and 200 W m^{-2}, respectively, with differences as large as 150 W m^{-2} (this region coincides with the location of the Gulf Stream). Near the low center, both OPNL and HSST show a small region of negative flux that would yield a damping effect on the storm's further development. Note that the zero line on the HSST forecast conforms to the coastline and then, eastward over the water, to the north wall of the Gulf Stream.

By 48 hours, the HSST experiment has a maximum heat flux more than twice as great as OPNL (Fig. 16). Maximum values are 150 and 350 W m^{-2} for OPNL and HSST, respectively, in approximately the same location. Both experiments show a negative heat flux of more than 100 W m^{-2} near the triple point, which by this time is located over relatively cold water.

2. Surface Moisture Flux

The difference in SST distribution affects not only the surface sensible heat flux but also the moisture flux. Since the moisture flux is

21

parameterized as being proportional to the difference between the saturation specific humidity corresponding to the SST and the low-level specific humidity in the atmosphere, results are similar to those for the surface sensible heat flux. At 24 h, the magnitudes of the maximum moisture flux west of the cold front were $71x10^{-6}$ and $89x10^{-6}$ kg m^{-2} s^{-1} for OPNL and HSST, respectively, in roughly the same location (Fig. 17). East of the cold front and south of the triple point, the magnitude of the moisture flux for HSST was about $10x10^{-6}$ kg m^{-2} s^{-1} higher than OPNL, providing more moisture in the warm sector of IOP-5 and a mechanism for increased latent heating. There was virtually no difference along the warm front itself.

By 36 h the moisture flux values and differences had increased, with maxima west of the cold front of $102x10^{-6}$ and $127x10^{-6}$ kg m^{-2} s^{-1} for OPNL and HSST (Fig 18). The gradient of the moisture flux just west of the cold front was stronger for HSST, providing another mechanism for heating and moistening the cold air more than the warm air. Frontal strength will be discussed in more detail when we examine the cross sections. In the warm sector east of the cold front, the moisture flux for HSST was again stronger than the OPNL by about $10x10^{-6}$ kg m^{-2} s^{-1}. Along the warm front, there was no difference. Both OPNL and HSST showed negative moisture fluxes near the low center, as was found for the heat flux at 36 h.

The differences at 48 h were smaller but still substantial, with maximum flux values west of the cold front of $99x10^{-6}$ and $119x10^{-6}$ kg m^{-2} s^{-1} for OPNL and HSST (Fig. 19). Both experiments showed negative moisture fluxes near the triple point just south of the warm front, which would

tend to damp further development there. However, both OPNL and HSST show positive fluxes further east, in the warm sector.

3.   950 mb Equivalent Potential Temperature (θ_e)

Equivalent potential temperature (θ_e) combines temperature and moisture parameters and so generally indicates fronts better than potential temperature alone. The 950 mb level is low enough within the MABL to be sensitive to the differences caused by surface fluxes between the three experiments.

At 24 hours, θ_e distributions at 950 mb along the cold front for all three experiments were similar (Fig. 20). NSF had a stronger cold front and was colder behind the cold front than OPNL and HSST (note the 290 K contour). Along the cold front, HSST had a weaker θ_e gradient than the other two experiments. This was due to the HSST having a stronger moisture flux west of the cold front. Surface fluxes act to heat and moisten the air behind the cold front to a greater extent than the air ahead of it. However, the HSST showed more warming along the warm front. The HSST 305 K contour extended further east near 60°W compared to OPNL, and NSF showed no eastward extension. This was due to the enhanced moisture flux in that region (Fig. 17).

By 36 hours, the differences in frontal strength continue to grow. The southward extension of the NSF cold front was much stronger than OPNL and HSST (Fig. 21), again due to the heating and moistening of the air west of the cold front by surface fluxes. Near the low center and along the warm front, the NSF showed the weakest gradient and HSST, the strongest.

23

At 48 hours, the OPNL and HSST θ_e distributions near the storm are nearly identical (Fig. 22). Again, the NSF experiment shows a tighter θ_e gradient along the cold front. By this time, the storm is fully occluded, as is indicated by the T-shaped θ_e distribution. While the NSF shows a stronger cold front, the OPNL and HSST show a stronger warm front. The tighter θ_e gradient north of the warm front coincides with positive heat and moisture fluxes (Figs. 16 and 19).

4. 950 mb Omega (ω)

Omega, the vertical motion in pressure coordinates, is sensitive to diabatic and frontal processes and so should reflect differences associated with surface fluxes. When sufficiently moist air moves upward to the condensation level, it releases latent heat into the atmosphere, which in turn increases upward motion. The low-level vertical gradient of omega is equivalent to low-level convergence and therefore provides for spin-up of the surface cyclone. The 950 mb vertical motion is examined in this section as an indicator of the effect of surface fluxes on the strength of the frontal circulations and low-level spin-up.

At 24 hours, the vertical motions at 950 mb for OPNL and HSST were similar in magnitude (4 μbar s^{-1}) and distribution (Fig. 23) with a maximum at the triple point and extensions along the warm and cold fronts. OPNL and HSST showed stronger velocity along the warm front, reflecting the stronger front as noted in the previous section. In contrast, NSF was slightly weaker in magnitude and showed only negligible upward motion in the vicinity of the warm front, as expected, given the relatively weak nature of the NSF warm front.

At 36 hours, the OPNL and HSST were again similar, with the NSF again showing less upward motion along the warm front (Fig. 24). The 2 μbar s^{-1} contour of the NSF extended further south along the cold front, since the cold front was stronger for the NSF than the other two experiments (as described above). Maximum values were similar for all three.

At 48 hours, the maximum upward motion was located at the triple point, with a magnitude of 6 μbar s^{-1} for OPNL and HSST and 5 μbar s^{-1} for NSF (Fig 25). All three experiments showed a similar vertical motion pattern along the fronts in a T-shape, indicating that the storm was occluded. While the differences along the cold front were negligible, stronger upward motion along the warm front indicates the stronger frontal strengths of OPNL and HSST, as expected due to the stronger frontal features described above.

5. Accumulated Precipitation

The precipitation accumulation over a 6 h period is a measure of the vertically integrated latent heat release averaged over 6 h. Three different precipitation fields were examined: convective, non-convective, and total. The non-convective or grid-scale precipitation is related to large-scale saturation which would be affected by both sensible heat and moisture fluxes. It is triggered when relative humidity (RH) exceeds saturation. The dependence on RH makes its response to surface fluxes complicated. If sensible heating warms the lower atmosphere, the RH will be decreased and less rain will occur. However, positive sensible heat fluxes are usually accompanied by positive moisture fluxes which increase

RH and precipitation. The convective precipitation is sensitive primarily to atmospheric stability and therefore to the sensible heat flux. In the NGM, convective precipitation is computed first, along with adjustments to the temperature and moisture fields. These adjustments in turn affect the non-convective precipitation. Of the three, significant differences were found for the convective and total; non-convective precipitation differences were smaller. As a result, the discussion will focus primarily on the convective precipitation.

At 24 h, the maximum convective precipitation was located near and south of the triple point with values of 146, 164, and 119 mm $6hr^{-1}$ for OPNL, HSST, and NSF, respectively (Fig 26). There was more precipitation for HSST along the warm front, due to increased warming, moistening, and therefore decreased stability along the warm front as described above. Interestingly, there were only negligible differences in total precipitation maxima for this forecast period: 163 for OPNL and 165 mm $6hr^{-1}$ for both HSST and NSF. Grid-scale (non-convective) precipitation compensated for the differences between the convective precipitation in the three experiments. This behavior was evident in the 36 h and 48 h forecasts as well.

By 36 h, a convective precipitation maximum was located near the low center with values of 237, 270, and 205 mm $6hr^{-1}$ for OPNL, HSST, and NSF (Fig 27). There was a slight difference in the location of the maximum precipitation: both the OPNL and HSST maxima were about 3° south and slightly west of the low center, while the maximum convective precipitation for NSF was located immediately west of the center. The maxima locations for OPNL and HSST coincided with the moisture flux maxima

26

(Fig 18), while the NSF maximum was forced primarily by RH and vertical motion. Maxima of total accumulated precipitation were 286, 297, and 258 mm 6hr^{-1} for the three forecasts, smaller differences than for the convective component, indicating that the grid-scale contribution again at least partially offset the large differences in convective precipitation. The total precipitation distributions were similar, with the maxima located just south and west of the storm's center.

At 48 hours, maximum convective precipitation values for OPNL and HSST were about 120 and 150 mm 6hr^{-1} with maxima located southwest of the storm center and the triple point (Fig 28). This precipitation distribution shows that by 48 hours there were two distinct regions of convection: near the triple point and one near the storm center. The NSF convective precipitation was weaker with a maximum value of 102 mm 6hr^{-1}. Total precipitation values for this forecast time were 196, 220, and 174 mm 6hr^{-1} for OPNL, HSST, and NSF. The grid-scale precipitation was the largest by this time. By 48 hours, RH exceeded saturation, and therefore non-convective precipitation increased. The decrease in convective precipitation was due to negative fluxes near the triple point. Note that even though moisture fluxes for OPNL and HSST were negative near the triple point, there is still convective precipitation due to strong upward motion combined with low-level moisture convergence (Figs 19 and 25).

B. CROSS SECTIONS

In this section, the vertical structure and frontal circulations of IOP-5 are further examined using cross sections. This discussion focusses on the 36 h forecast, which is midway through the rapid deepening phase of

27

IOP-5. Figure 29 is the 36 h OPNL forecast of sea level pressure and 300 mb wind speed. It suggests a possible dynamic interaction between two jet streaks as described by Uccellini and Kocin (1987). Three cross sections (AB, CD, and EF) are shown in Figure 29. Cross section AB is perpendicular to the cold front and passes through the region of maximum heat flux in the cold air mass west of the front as well as the maximum upward vertical velocity associated with the cold front. Cross section CD passes through the low center, southward through the cold air mass, then diagonally across the cold front. Cross section EF runs perpendicular to the warm front, then through the cold front twice. Cross sections CD and EF both transect the jet streak located south of the surface low.

Figures 30 - 32 show the AB cross sections for the three experiments with potential temperature (θ) and omega (ω) contours and ageostrophic wind vectors in the plane of the cross section. These cross sections reveal that the region near the cold front was warmer for the OPNL and HSST experiments than for NSF. Note the 290K contour runs into the surface at the cold front for OPNL and HSST, while remaining at about the 950 mb level for NSF. HSST was colder than OPNL in the center of the cold air (note 280K isentrope), but appears to be warmer near the cold front (note 288K isentrope). Upward vertical motion was strongest for OPNL, with a maximum ω of 8 μbar s^{-1} near the 800 mb level associated with the cold front. HSST and NSF showed a maximum ω of 7 μbar s^{-1}, with HSST stronger, showing a larger 7 μbar s^{-1} contour than NSF. HSST shows the strongest downward vertical motion near the 850 mb level immediately west of the cold front, with 3 μbar s^{-1} compared to 2 μbar s^{-1} for OPNL and 1 μbar s^{-1} for NSF. Downward motion was slightly less for NSF in the upper

28

troposphere west of the front. Note that the 4 μbar s^{-1} contour that is present for both OPNL and HSST at 450 mb level in the center of the figure is missing for NSF. The thermal structure above 700 mb is very similar for all three experiments.

Cross section CD passes through the low center; the strong upward vertical motion marks the storm's location (Figs 33 - 35). Stability near the surface, south of the low, is lowest for HSST (Fig 34) as indicated by the spacing between the isentropes. HSST shows a tighter horizontal θ gradient in the low center, and a weaker gradient in the cold air to the north. The low center is located very near the north wall of the Gulf Stream; the HSST experiment has warmer surface water than OPNL, and the increased air-sea temperature difference in turn influences the surface fluxes as mentioned above. OPNL shows the strongest upward motion above the storm, with a maximum ω of 17 μbar s^{-1} at 600 mb, compared to 15 μbar s^{-1} for HSST and NSF. South of the storm, the descent maximum of 4 μbar s^{-1} for OPNL and HSST was twice that of NSF.

Low-level horizontal winds above the low center were the weakest for HSST, with wind speeds less than 10 m s^{-1} in a cone-shaped minimum positioned over the low (Figs 36 - 38). OPNL was similar to HSST, but NSF did not drop below 10 m s^{-1} over the low. Some differences in winds were apparent up to 500 mb in this cross section, but not above that level. Since the thermal structures between the three experiments are similar, geostrophic winds should also be similar. Therefore, differences in wind speeds must be due to a combination of the ageostrophic wind component near the upward motion maxima.

Cross section EF is perpendicular to the warm front through the upward motion maximum. The HSST experiment was warmer than OPNL and NSF over the warm front throughout the column extending up to 300 mb. South of the warm front, the isentrope spacing suggests the lowest stability in the boundary layer for OPNL; HSST had a similar pattern to OPNL, and NSF was the most stable of the three experiments (Figs 39 - 41). The Gulf Stream appears to cause the stronger front for HSST as shown by the stronger horizontal θ gradient north of the warm front. The upward vertical motion was strongest at the warm front for HSST (25 μbar s^{-1}), with OPNL and NSF showing 22 and 18 μbar s^{-1}, respectively. This contrasts with OPNL having the greatest vertical motion for cross sections AB and CD above the cold front and the low center. HSST shows a small region of descent at 650 mb, just south of the warm front; neither the OPNL nor NSF depicted this feature. This indicates a stronger frontal circulation, due to the stronger thermal gradient caused by the underlying high resolution SST. There is a wind speed minimum for HSST located just south of the warm front (Figs 42 - 44); this minimum does not appear in OPNL or NSF. With that exception, there is little difference between the three experiments with respect to isotach distribution.

VI.   CONCLUSIONS AND RECOMMENDATIONS

A.   CONCLUSIONS

For ERICA IOP-5, the effects of a high resolution SST in the NGM were at best only subtle in synoptic-scale features.   Storm movement and central pressure forecasts were similar between the three experiments. A combination of the NGM resolution and the MABL parameterization probably caused a smoothing of many of the smaller scale features.

The high resolution SST affected mainly low-level processes.   Most notable were the surface fluxes, with the HSST showing higher fluxes in the cold air region of the storm due to larger air-sea temperature differences associated with the Gulf Stream.   However, even though there were large differences in fluxes between HSST and OPNL, both had the same central pressure forecast at 48 h.

The vertical structure and frontal circulations were more detailed with the HSST.   Upward motion along the warm front was enhanced by the position of the Gulf Stream below.   This produced differences in convective and total precipitation, with the HSST precipitation amounts higher than OPNL and NSF.   The OPNL showed stronger upward motion at the cold front itself, while the HSST showed stronger downward motion just west of the front.

In any forecasting situation, one must begin with an accurate analysis.   During ERICA, there was an abundance of data collected from many different platforms in a region which is usually considered "data

31

sparse". In normal situations, an analysis which may not be so accurate is used to initialize the NGM. Given this typical lack of data, perhaps a high resolution SST would have a more significant impact on a normal operational NGM forecast cycle.

B. RECOMMENDATIONS

1. This paper has focussed on the effects of a high resolution SST on the NGM. Since the effect on this scale of a forecasting model was small, further studies of high resolution SST should be performed on mesoscale models with higher resolution.

2. Input the higher resolution SST into the same model using different MABL parameterizations. Surface fluxes as analyzed by Greer (1991) were significantly higher than the experimental forecast fluxes in the warm sector of IOP-5 during and prior to rapid cyclogenesis. In the warm sector, the 24h forecast (the beginning of rapid cyclogenesis) sensible heat fluxes for OPNL and HSST were approximately 10 and 50 W m^{-2}, respectively, compared to Greer's analyzed flux, which was greater than 200 W m^{-2}. If the experimental models had forecast fluxes of that magnitude, perhaps synoptic-scale predictions would be different since the fluxes enhance destabilization of the MABL. It is conceivable that the MABL package for the NGM simply did not respond to the variation and gradients of the higher resolution SST, or simply damped out effects that may have occurred.

3. In this paper, the OPNL and HSST were compared to determine the effect of a high resolution SST on forecasted parameters. However, two different surface exchange coefficients were used, the one for the HSST being a more sensitive (and now operational) coefficient. For further studies with smaller scale models, recommend using the same surface exchange coefficient, so that the coefficient itself does not become another variable.
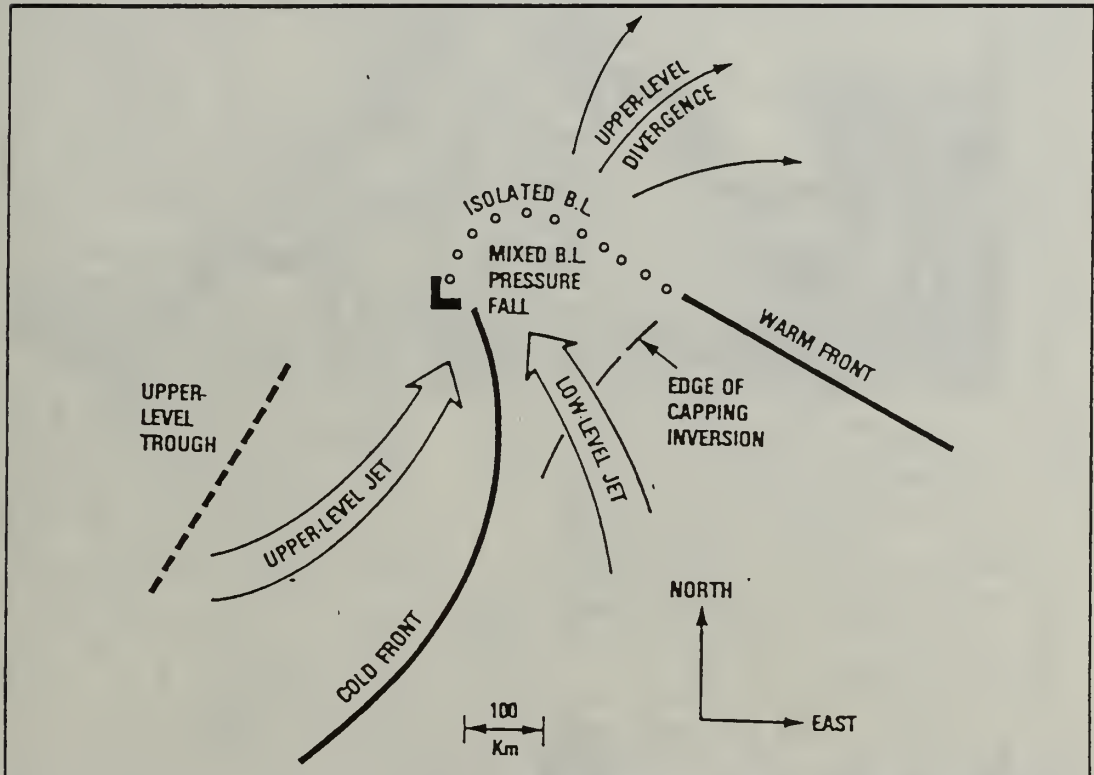
Figure 1. Scale Interaction Schematic for Rapid Marine Cyclogenesis (Hadlock and Kreitzberg 1988)
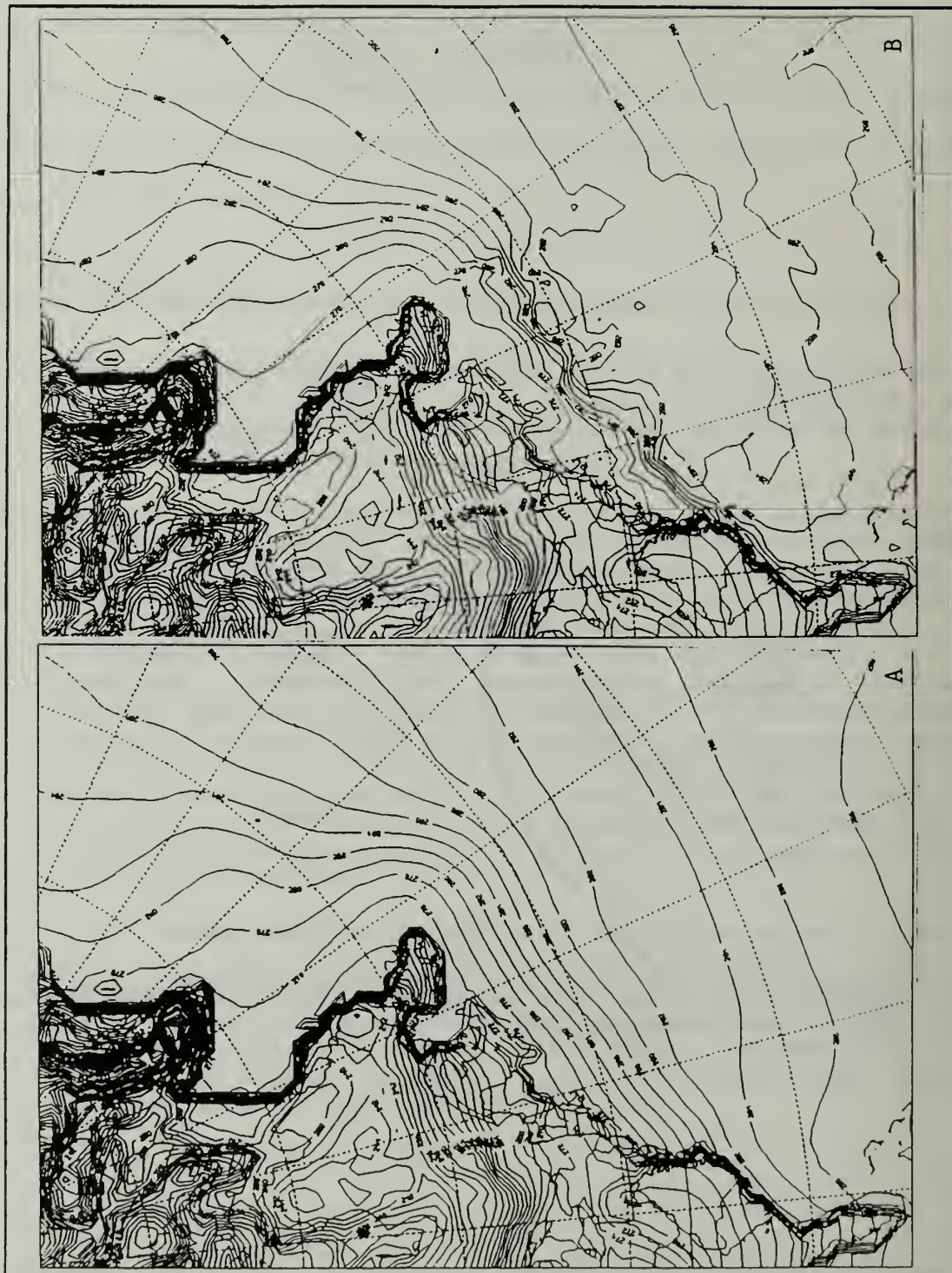
Figure 2. Sea Surface Temperature (SST) Analyses: (A) Global blended
SST (K), 2° x 2° spacing; (B) NOAA/NESS MCSST (K), .5° x .5° spacing
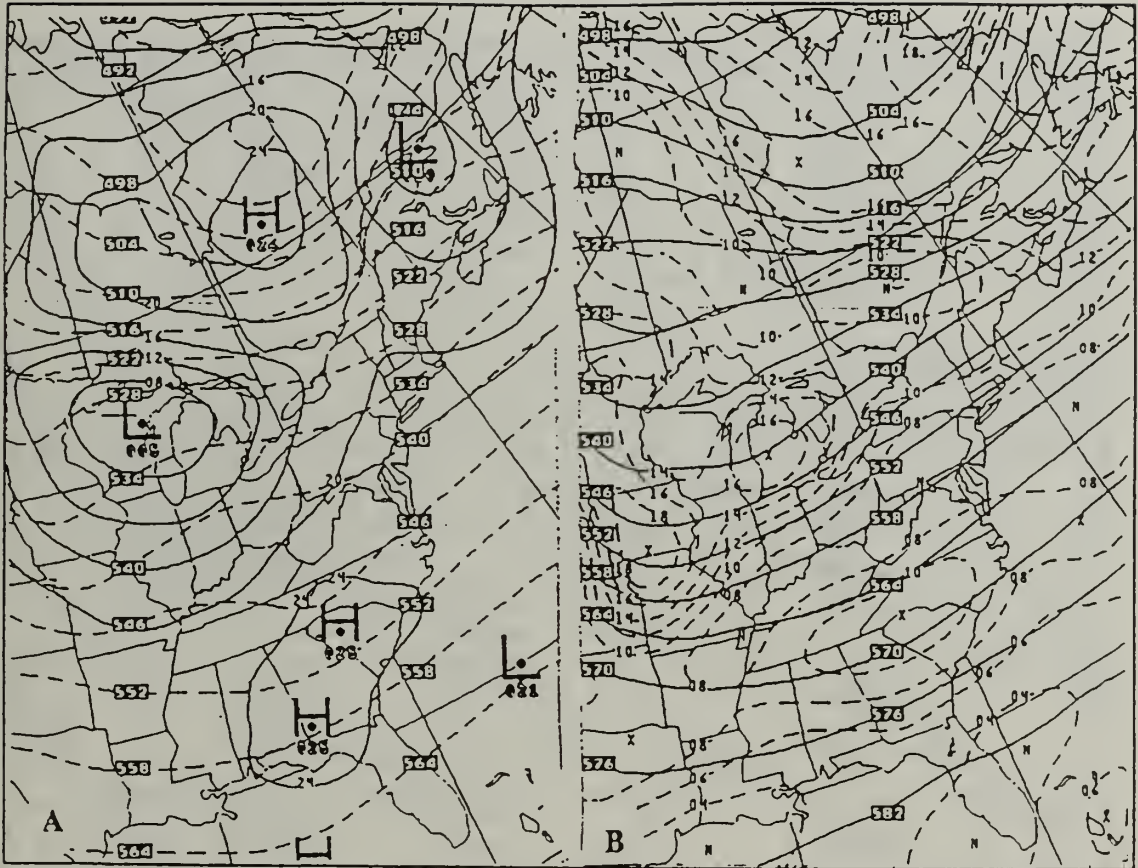
Figure 3. NGM Analyses, 12Z/18: Sea level pressure (mb; solid) and
1000-500 mb thickness (dm; dashed); (B) 500 mb heights (dm; solid)
and absolute vorticity (10^{-5} s^{-1}; dashed)

35
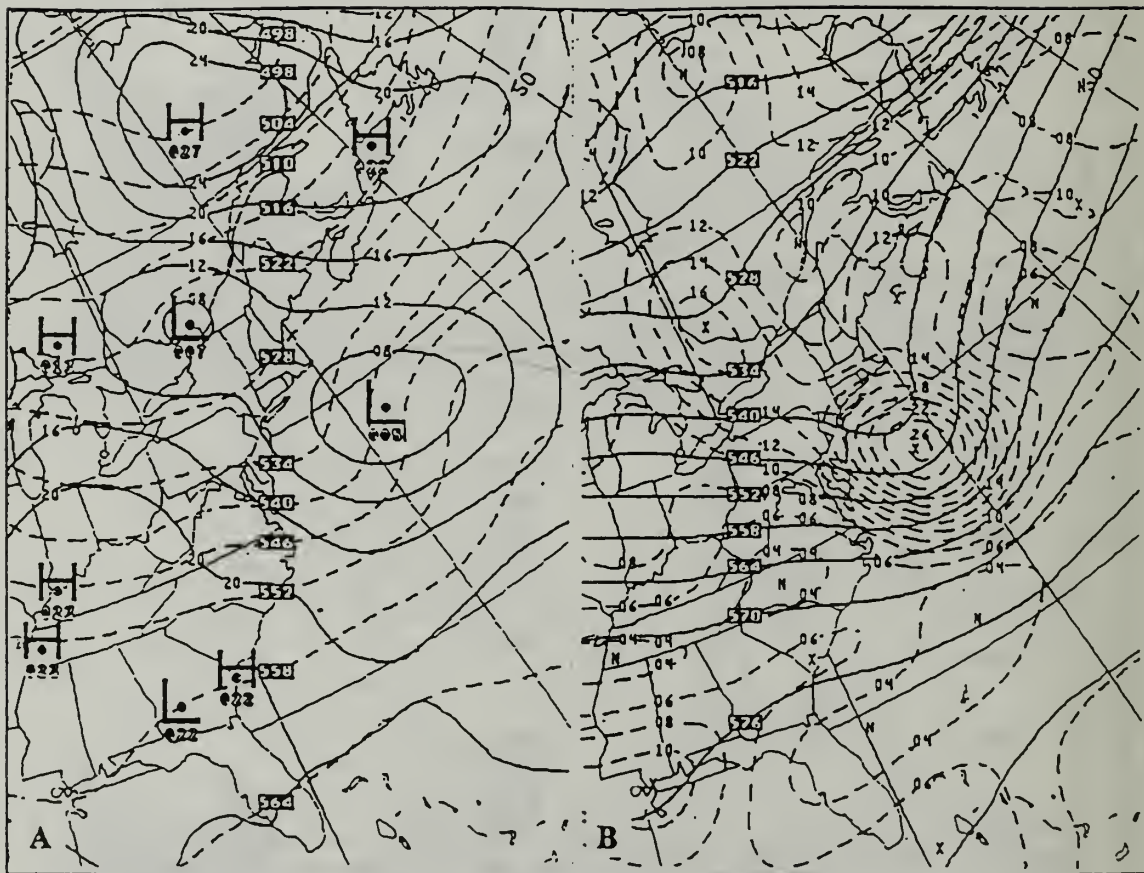
Figure 4. As in Fig. 3, except 12Z/19
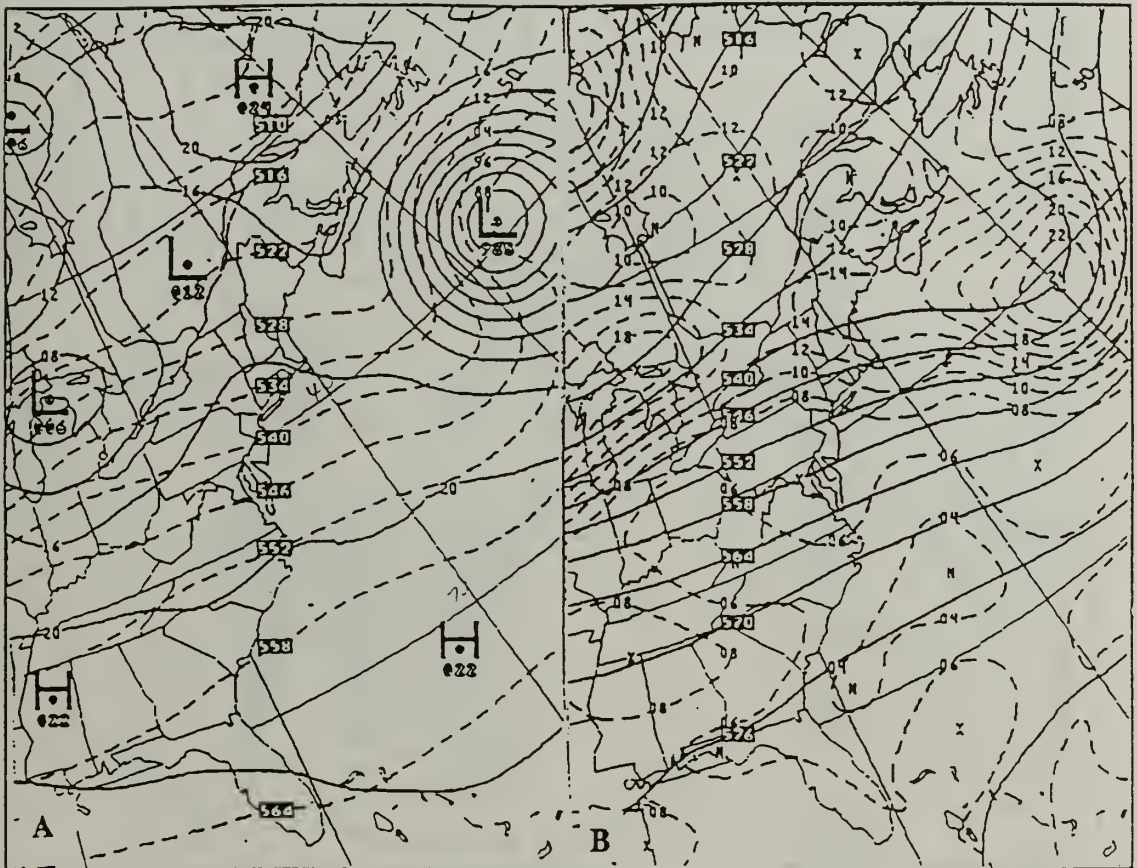
Figure 5. As in Fig. 4, except 00Z/20
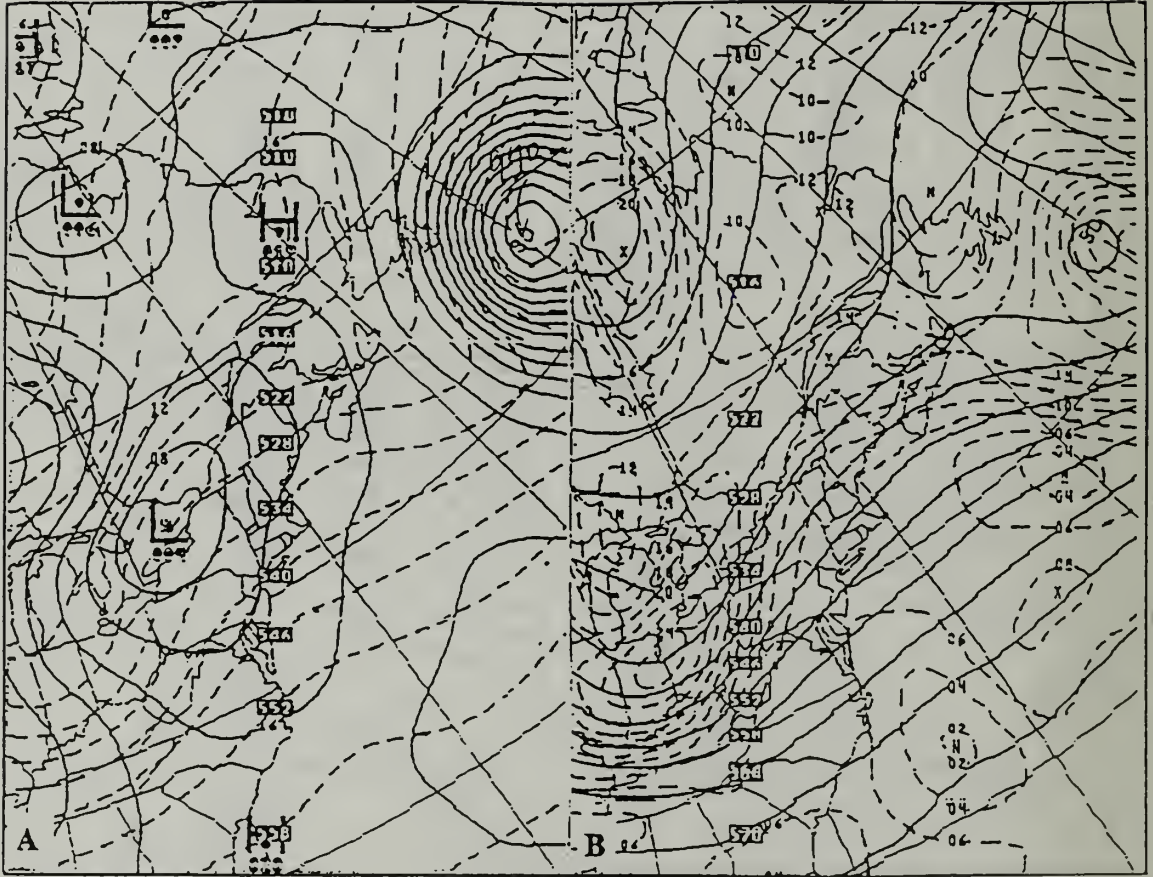
Figure 6. As in Fig. 5, except 12Z/20
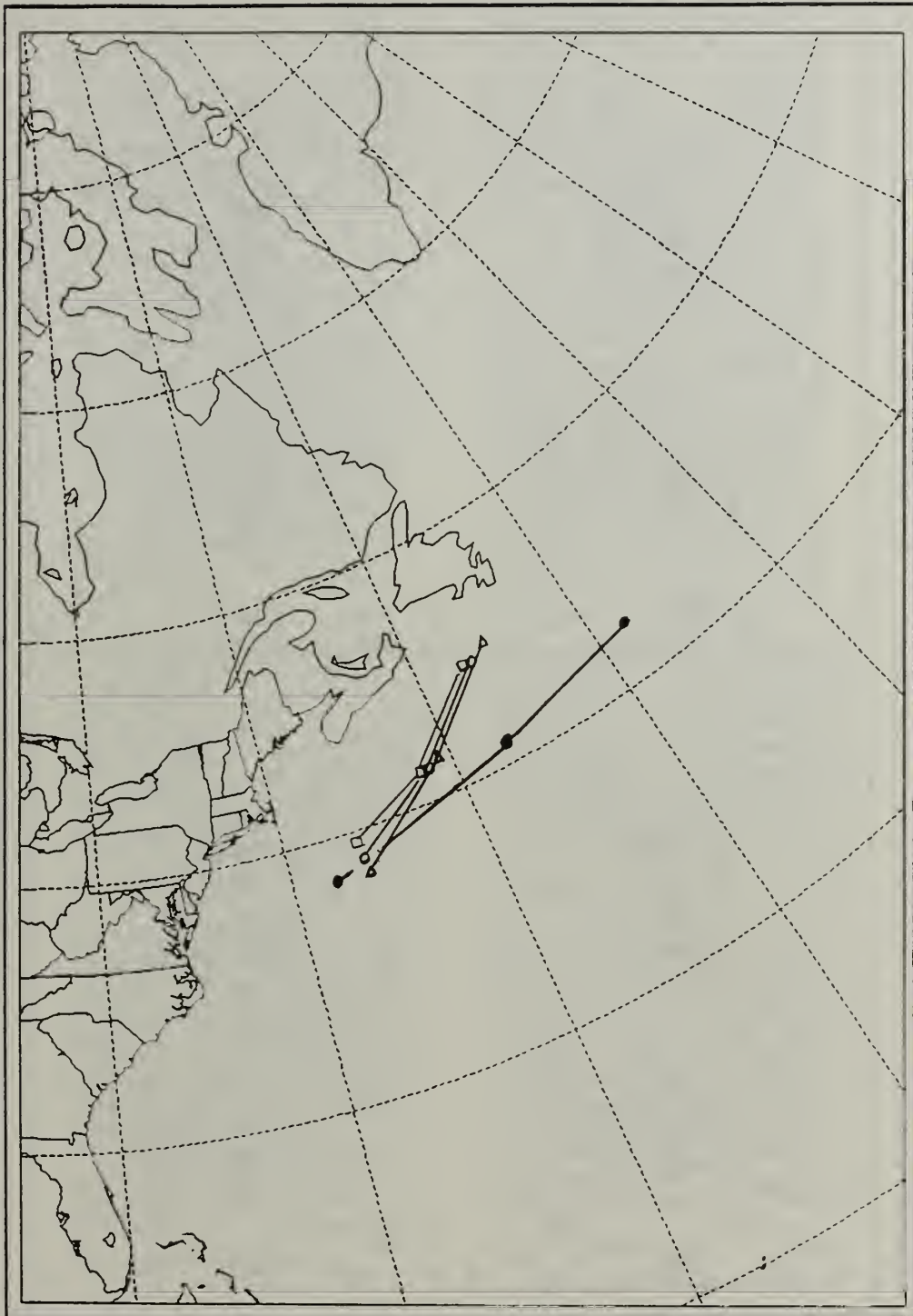
Figure 7. Storm tracks for ERICA IOP-5: Observed (solid), OPNL forecast (bold dashed), HSST forecast (dash dot), NSF forecast (dotted)
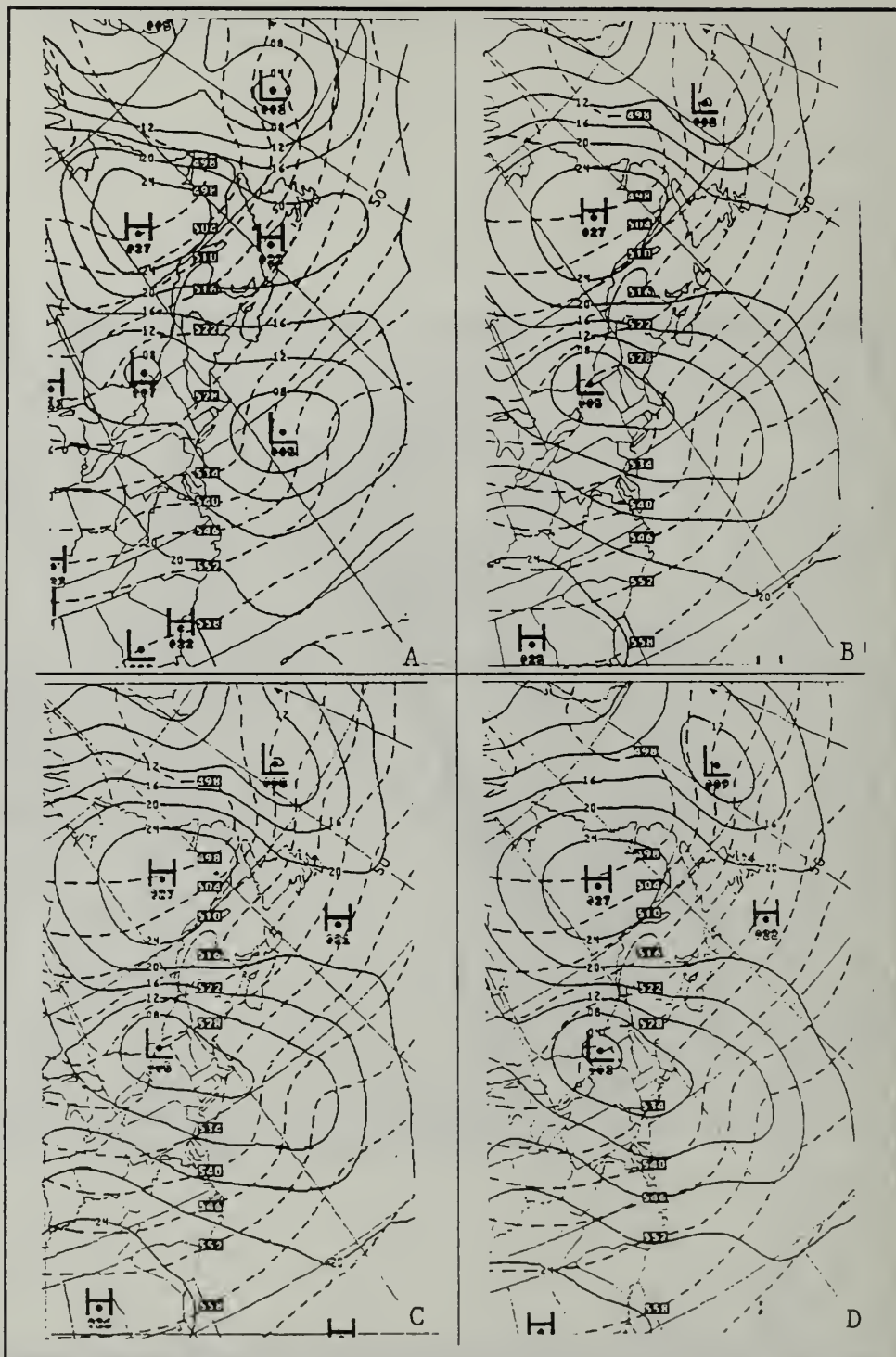
Figure 8. NGM surface analysis with 24 h forecasts, VT
12Z/19: (A) NGM analysis; (B) OPNL forecast; (C) HSST
forecast; (D) NSF forecast. Units as in Fig. 3A

Figure 9. NGM 500 mb analysis with 24 h forecasts, VT
12Z/19: (A) NGM analysis; (B) OPNL forecast; (C) HSST
forecast; (D) NSF forecast. Units as in Fig. 3B

41
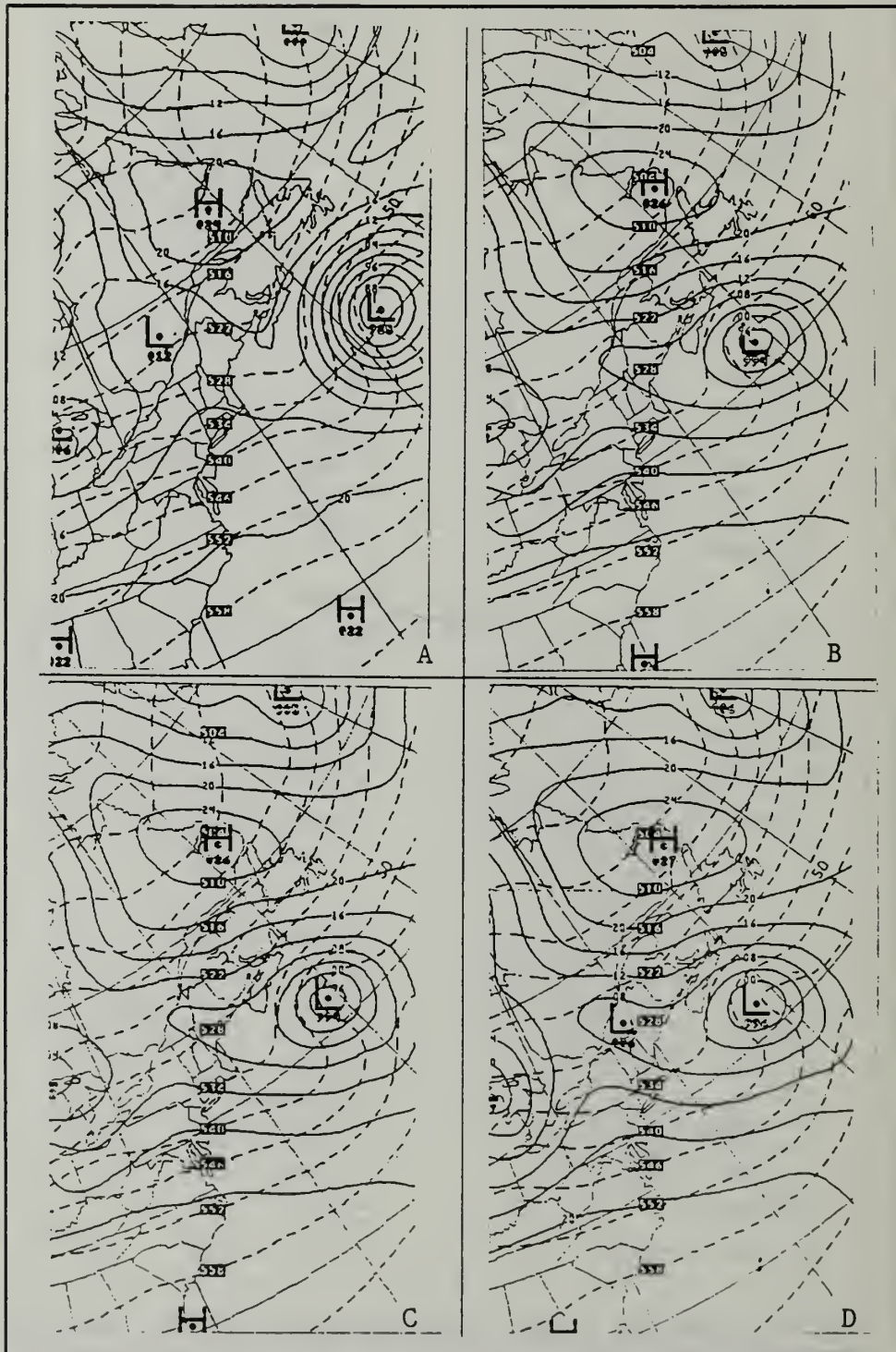
Figure 10. As in Fig. 8, except 36 h forecast, VT 00Z/20
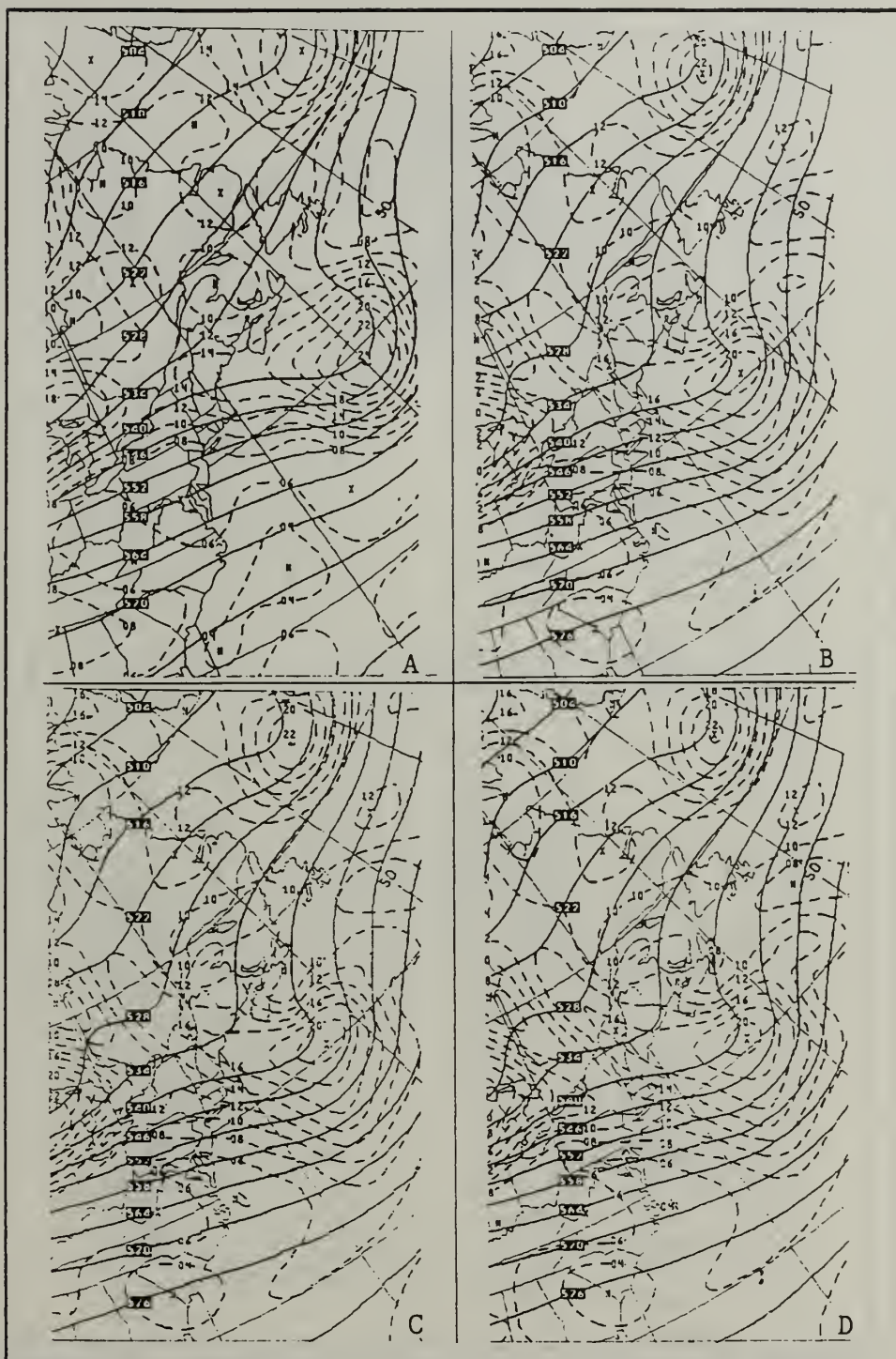
Figure 11. As in Fig. 9, except 36 h forecast, VT 00Z/20
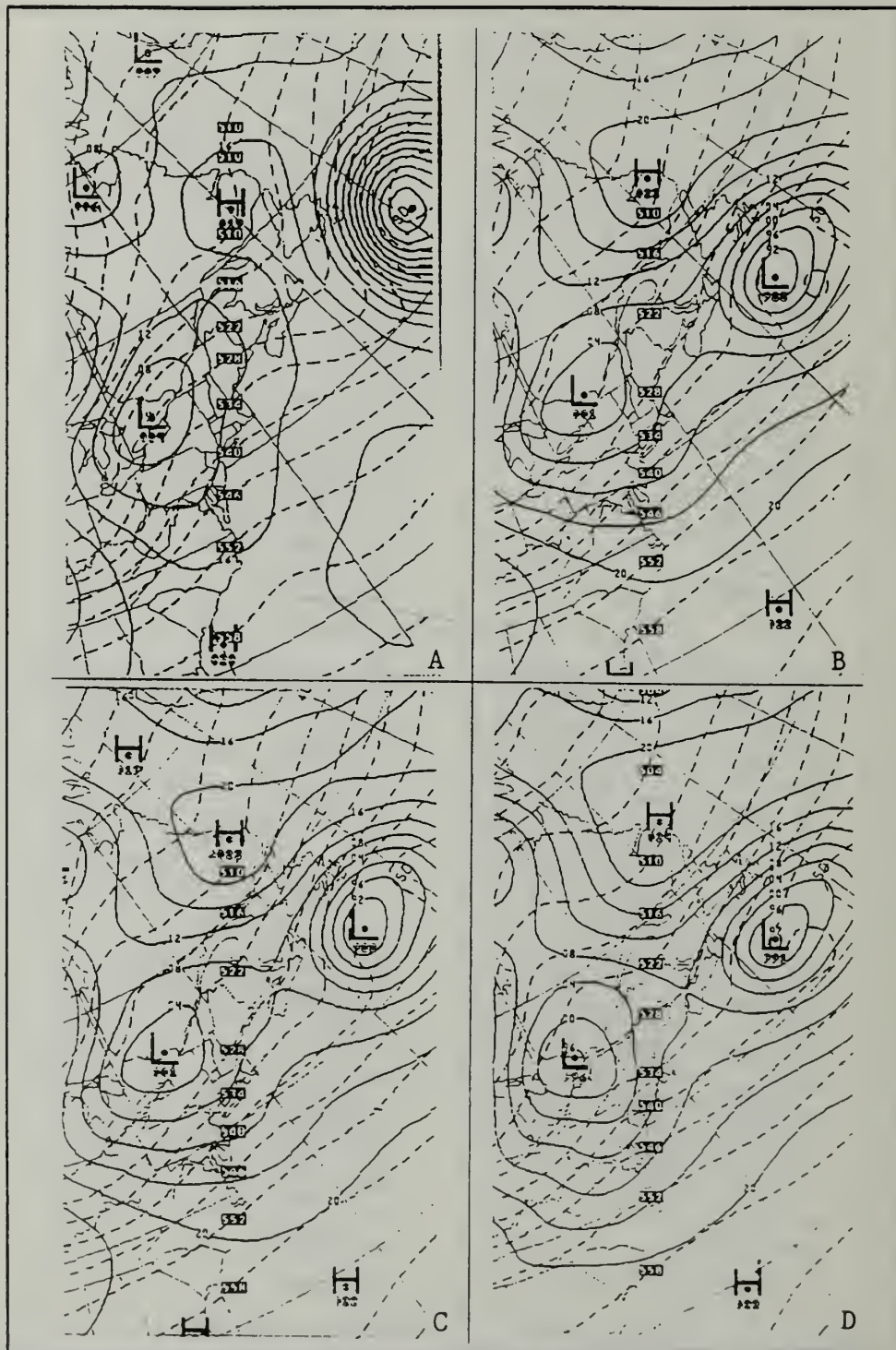
Figure 12. As in Fig. 8, except 48 h forecast, VT 12Z/20
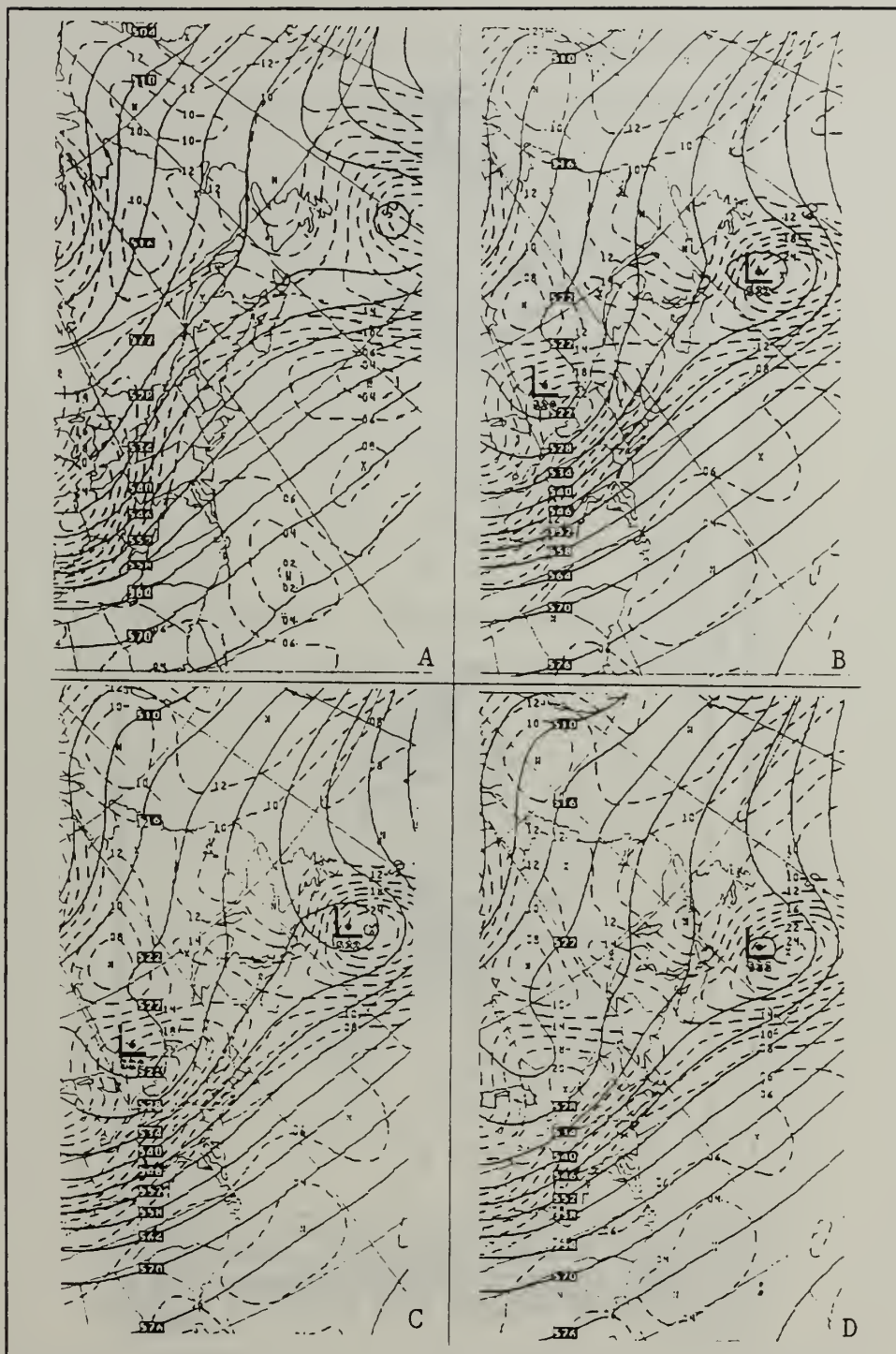
Figure 13. As in Fig. 9, except 48 h forecast, VT 12Z/20

45
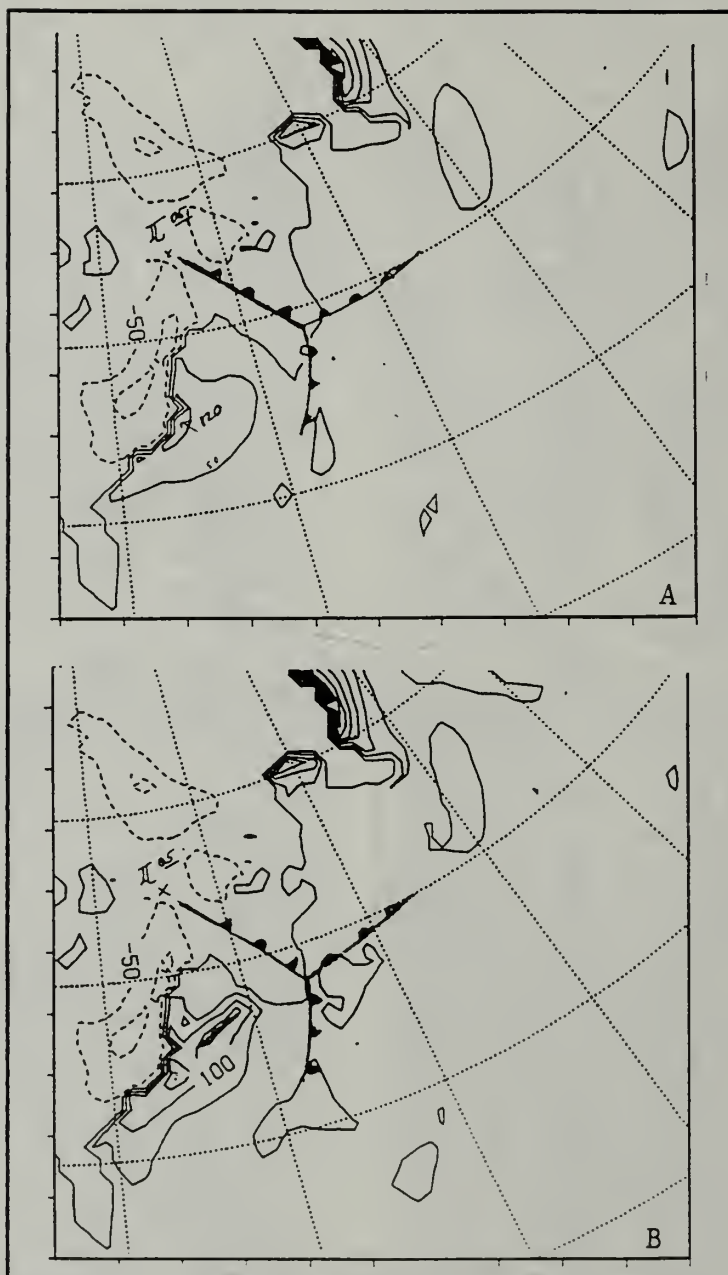
Figure 14. Sensible Heat Flux, 24 h forecast:
(A) OPNL forecast; (B) HSST forecast. 50 W
m^{-2} increment (dashed line indicates negative
flux)
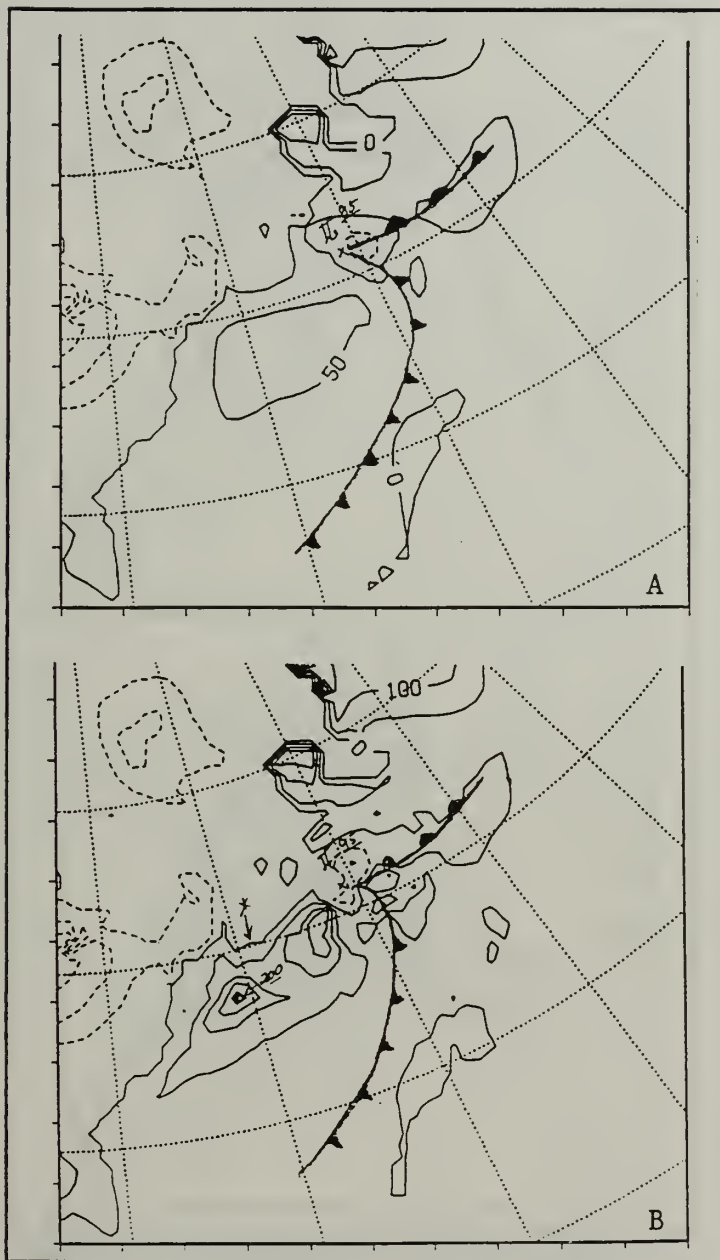
Figure 15. As in Fig. 14, except 36 h forecast

47
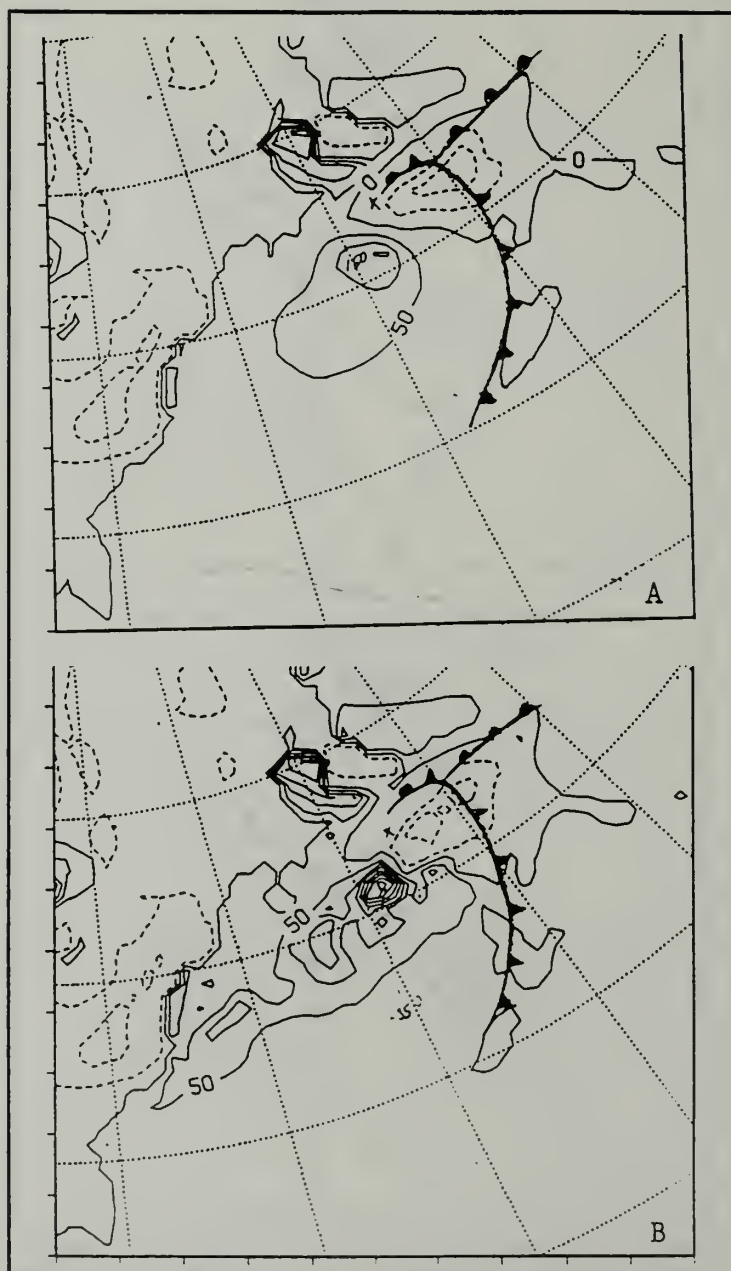
Figure 16. As in Fig. 14, except 48 h
forecast

48
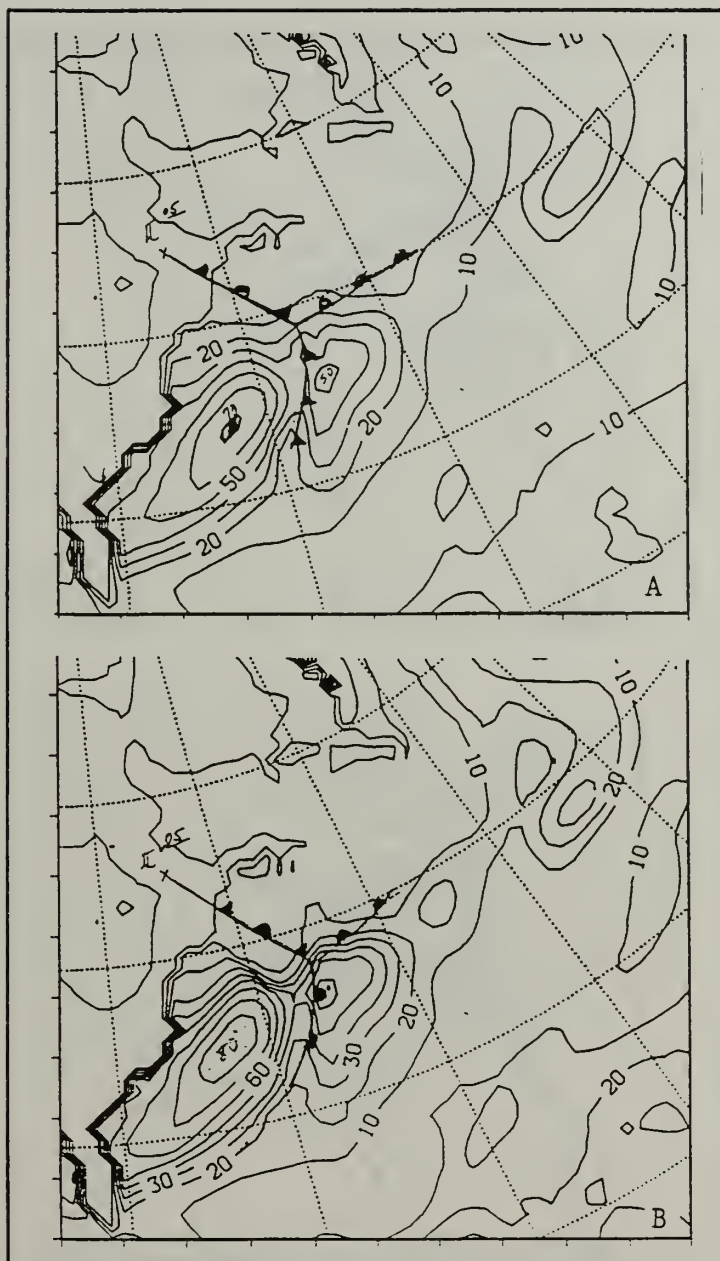
Figure 17. Surface Moisture Flux, 24 h
forecast: (A) OPNL forecast: (B) HSST
forecast. 10×10^{-6} kg m^{-2} s^{-1} increment
(dashed line indicates negative flux)
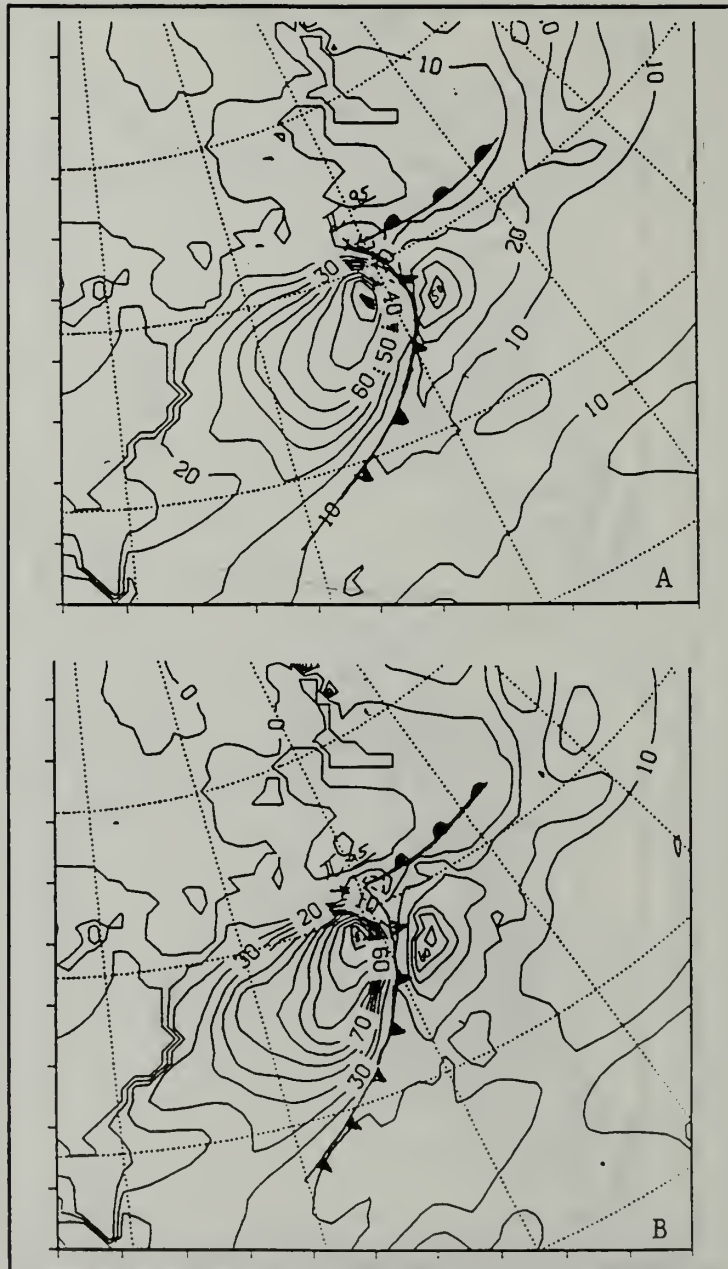
Figure 18. As in Fig. 17, except 36 h forecast
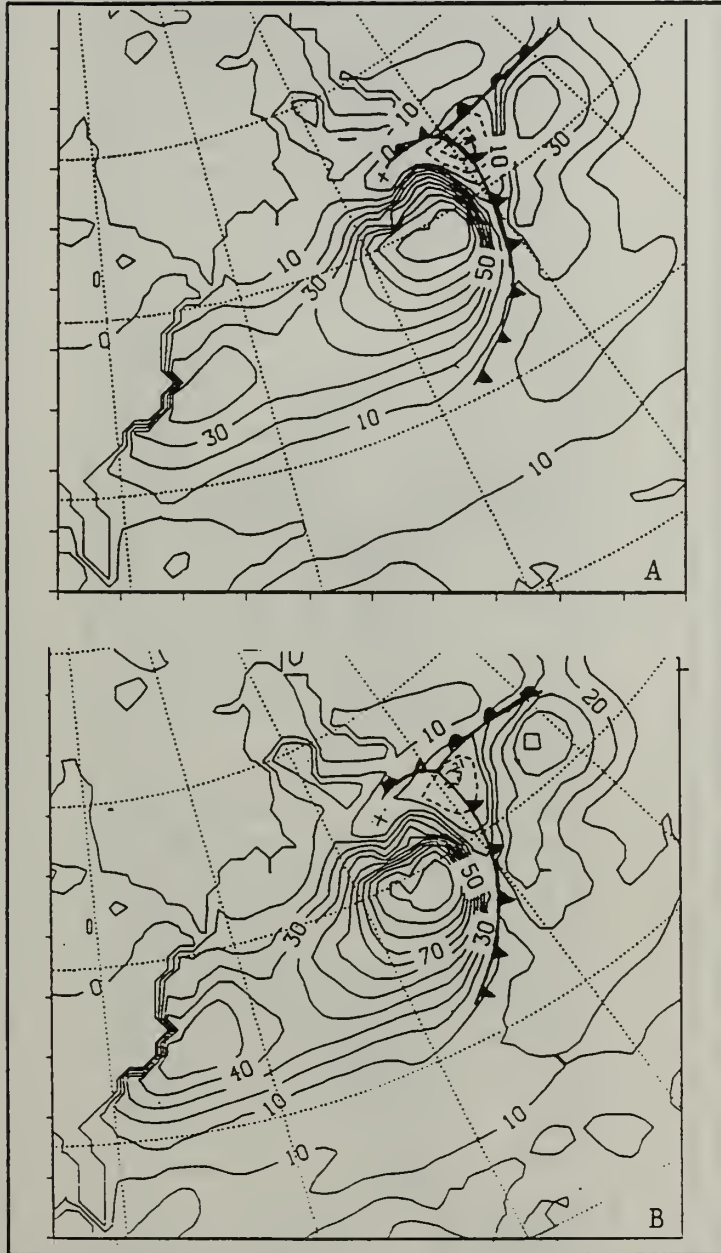
Figure 19. As in Fig. 17, except 48 h forecast
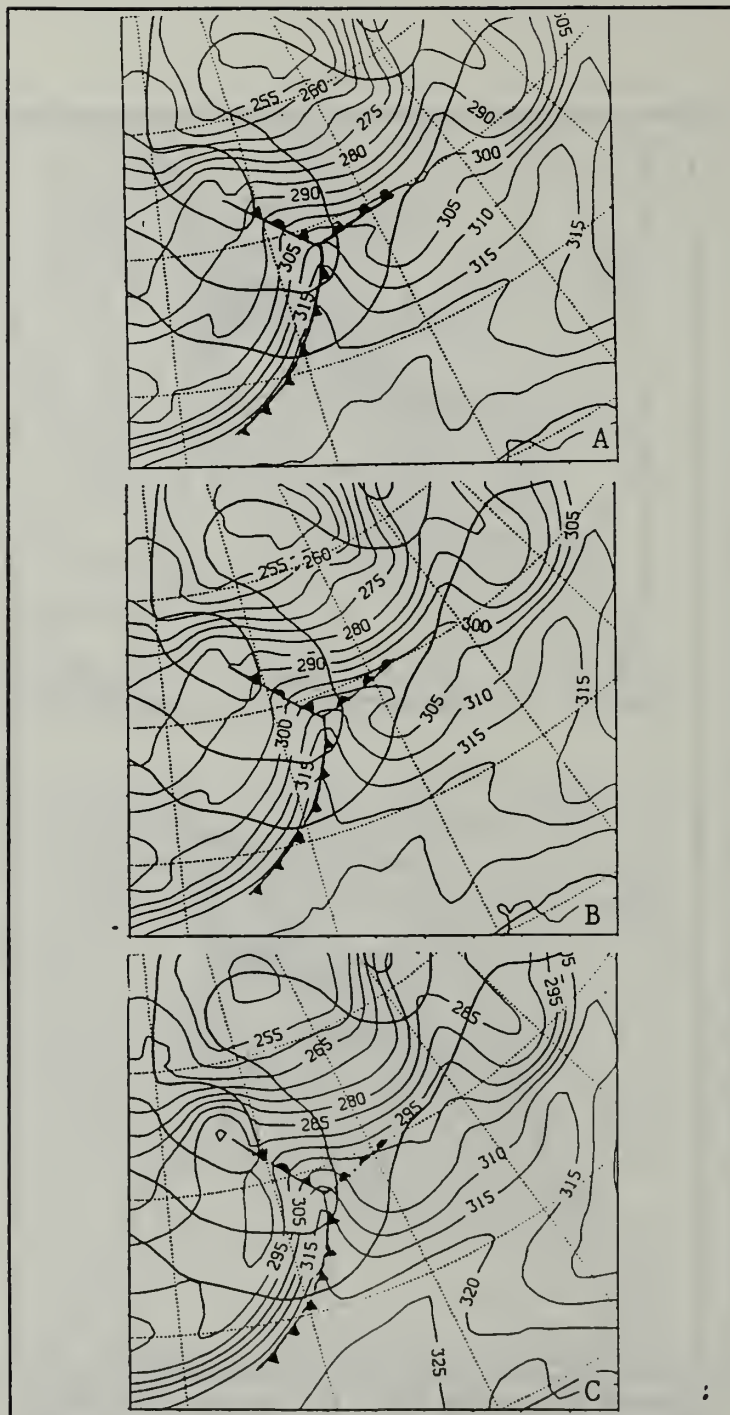
Figure 20. 950 mb Equivalent Potential
Temperature, 24 h forecast: (A) OPNL; (B)
HSST; (C) NSF forecast. Temperature (thin) 5
K increment; heights (bold) 30 dm increment

52
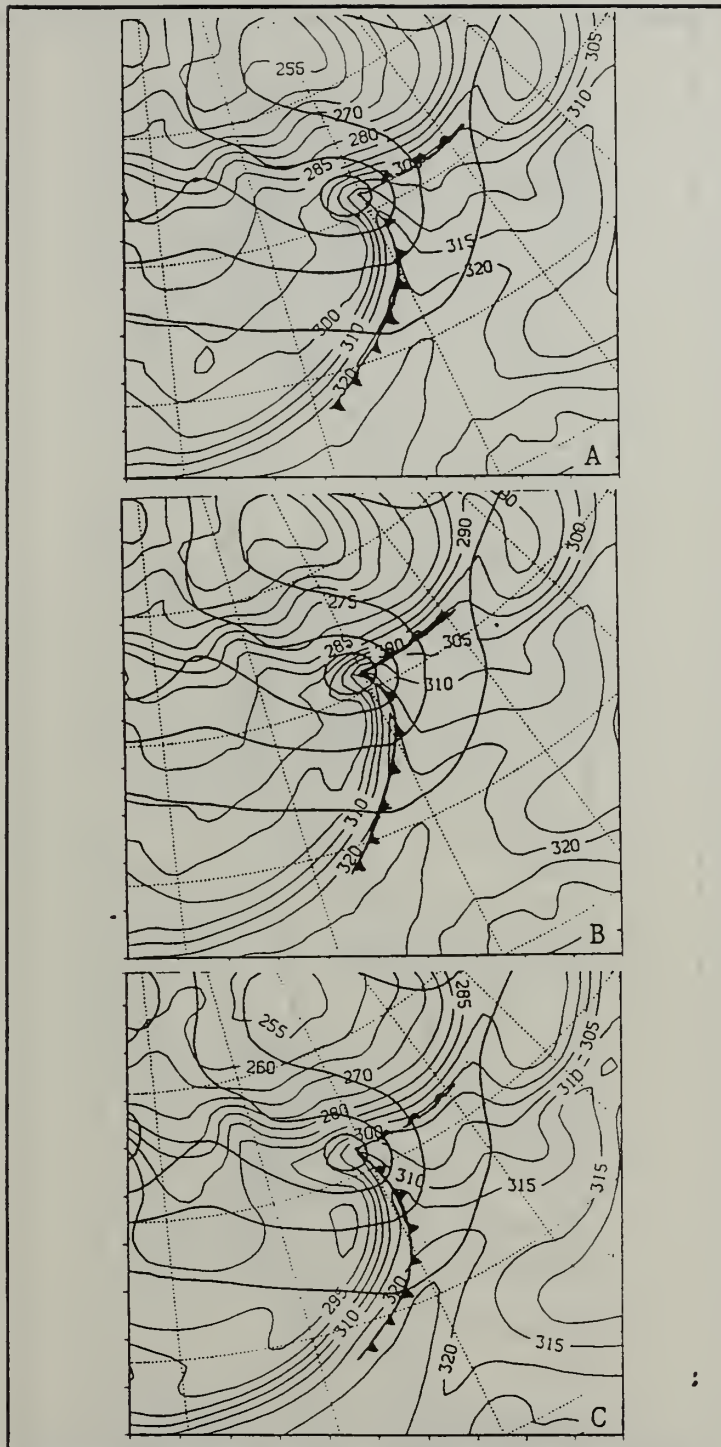
Figure 21. As in Fig. 20, except 36 h
forecast
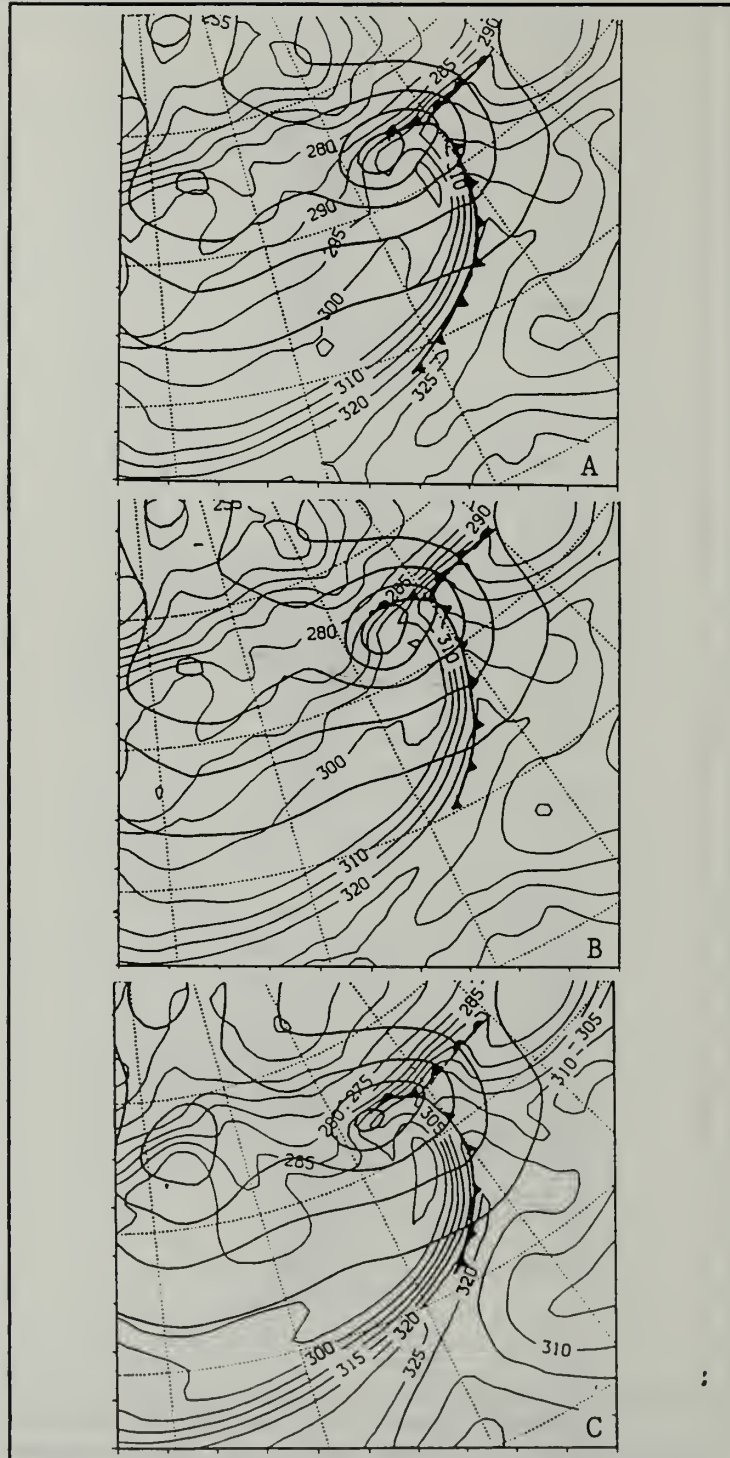
Figure 22. As in Fig. 20, except 48 h
forecast
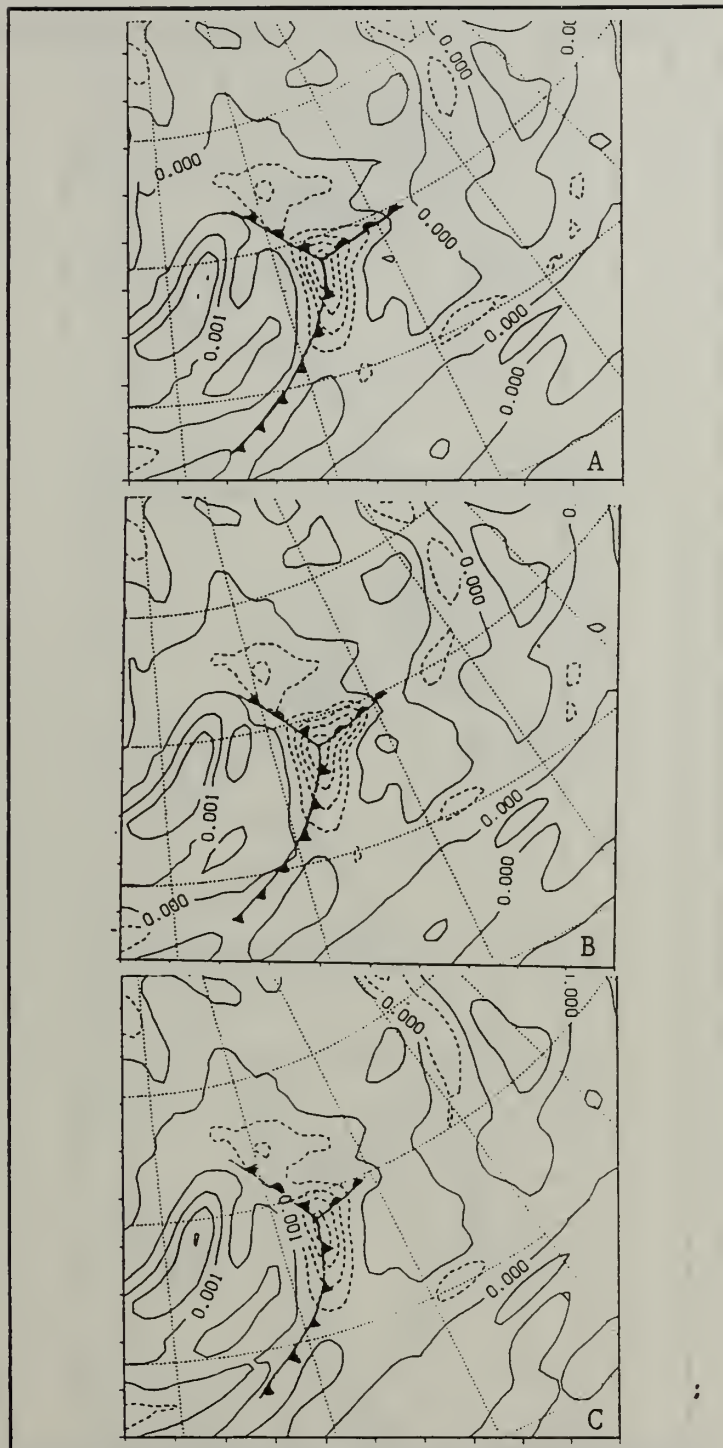
Figure 23. Vertical Velocity, 24 h forecast:
(A) OPNL; (B) HSST; (C) NSF. 1 μbar s^{-1}
increment
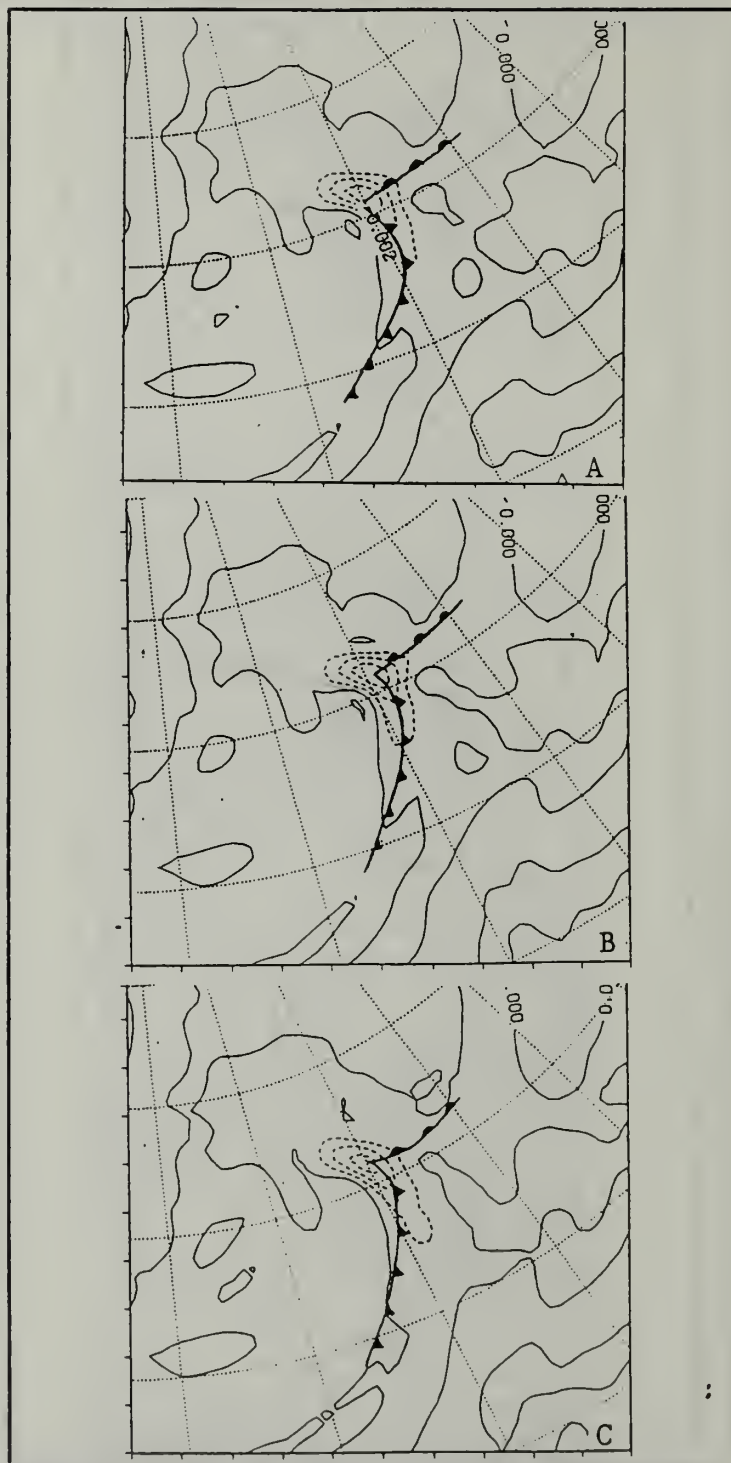
Figure 24. As in Fig. 23, except 36 h
forecast. 2 μbar s^{-1} increment

56
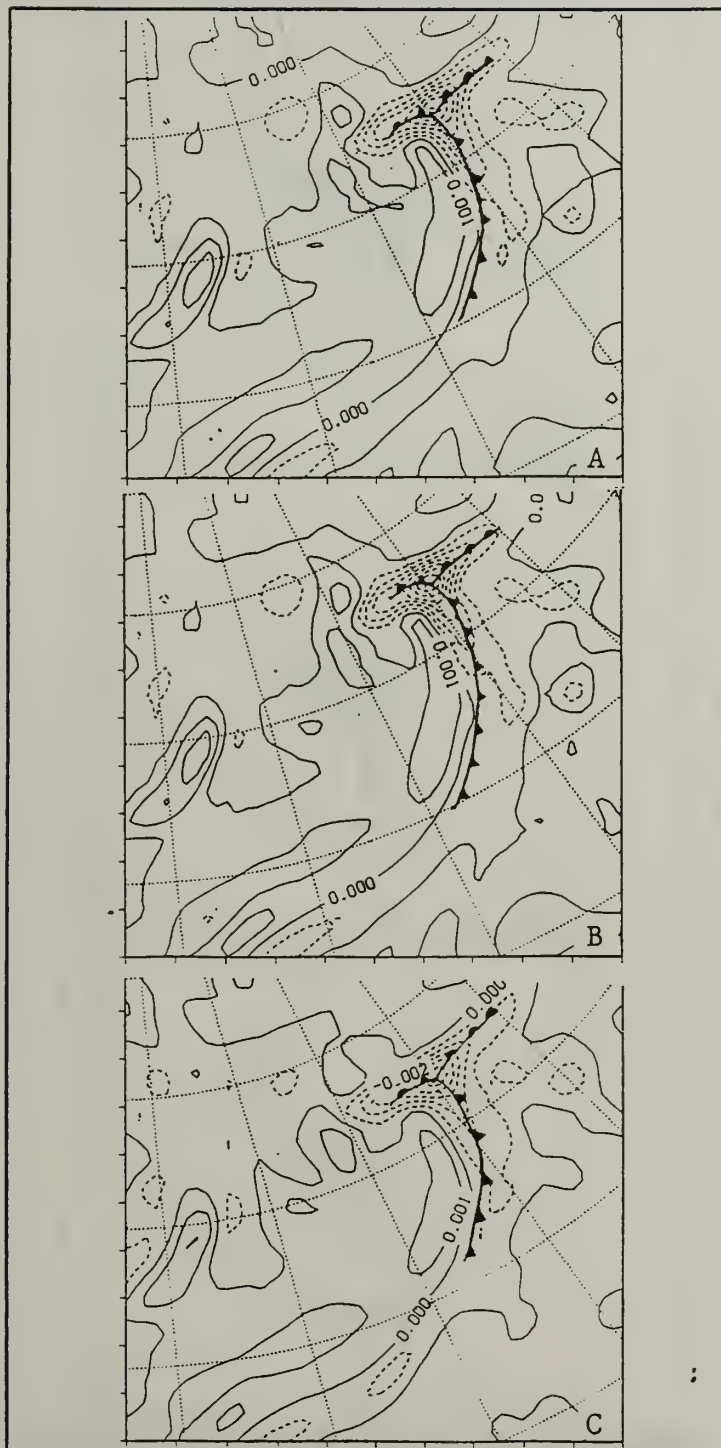
Figure 25. As in Fig. 23, except 48 h
forecast. 1 μbar s^{-1} increment
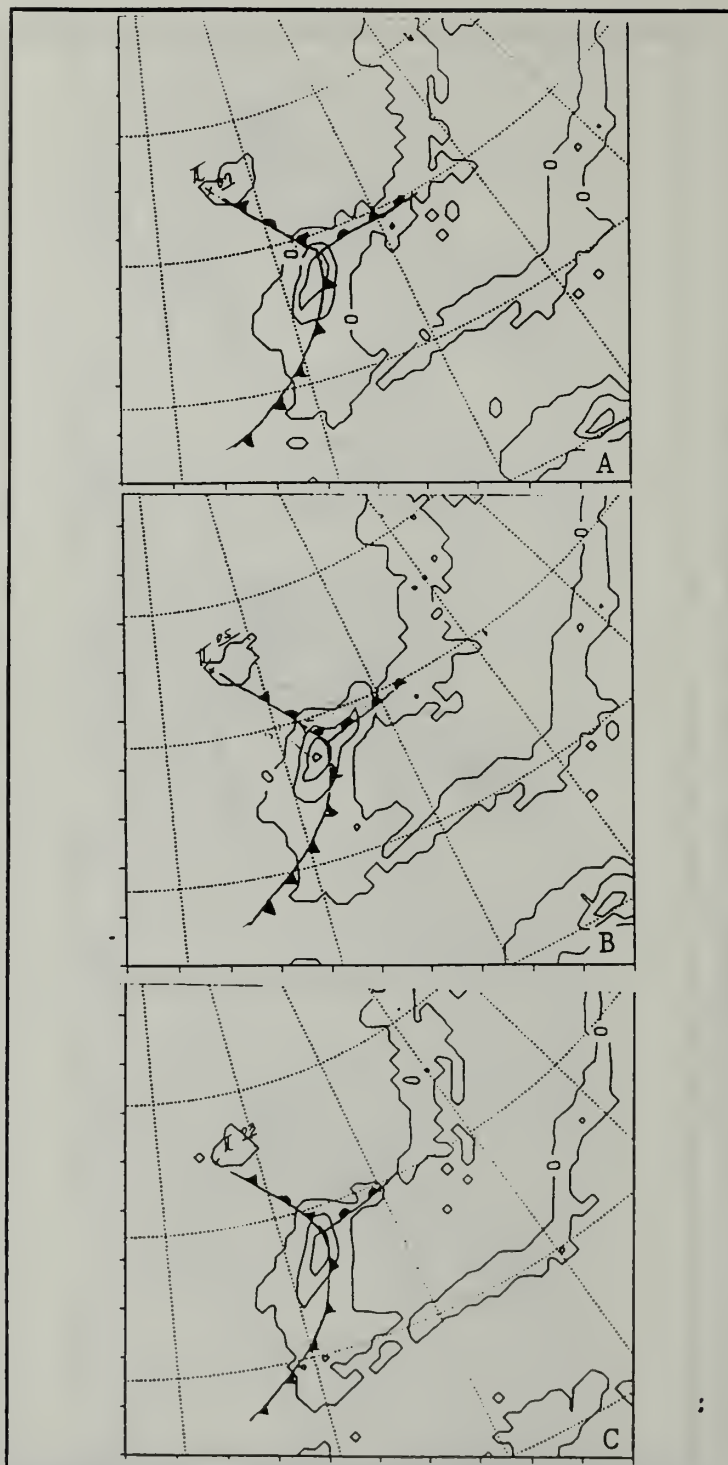
Figure 26. Convective Precipitation, 24 h
forecast: (A) OPNL; (B) HSST; (C) NSF. 50 mm
$6hr^{-1}$ increment
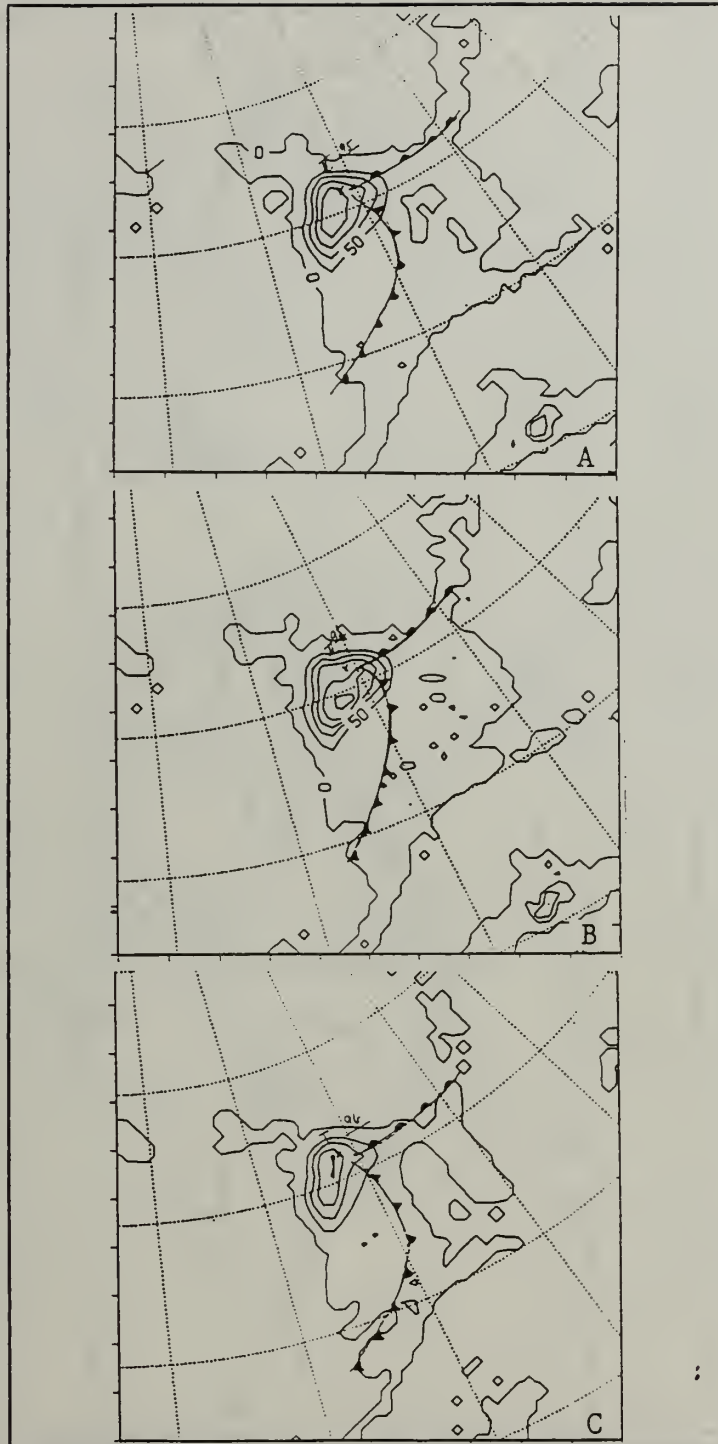
Figure 27. As in Fig. 26, except 36 h
forecast
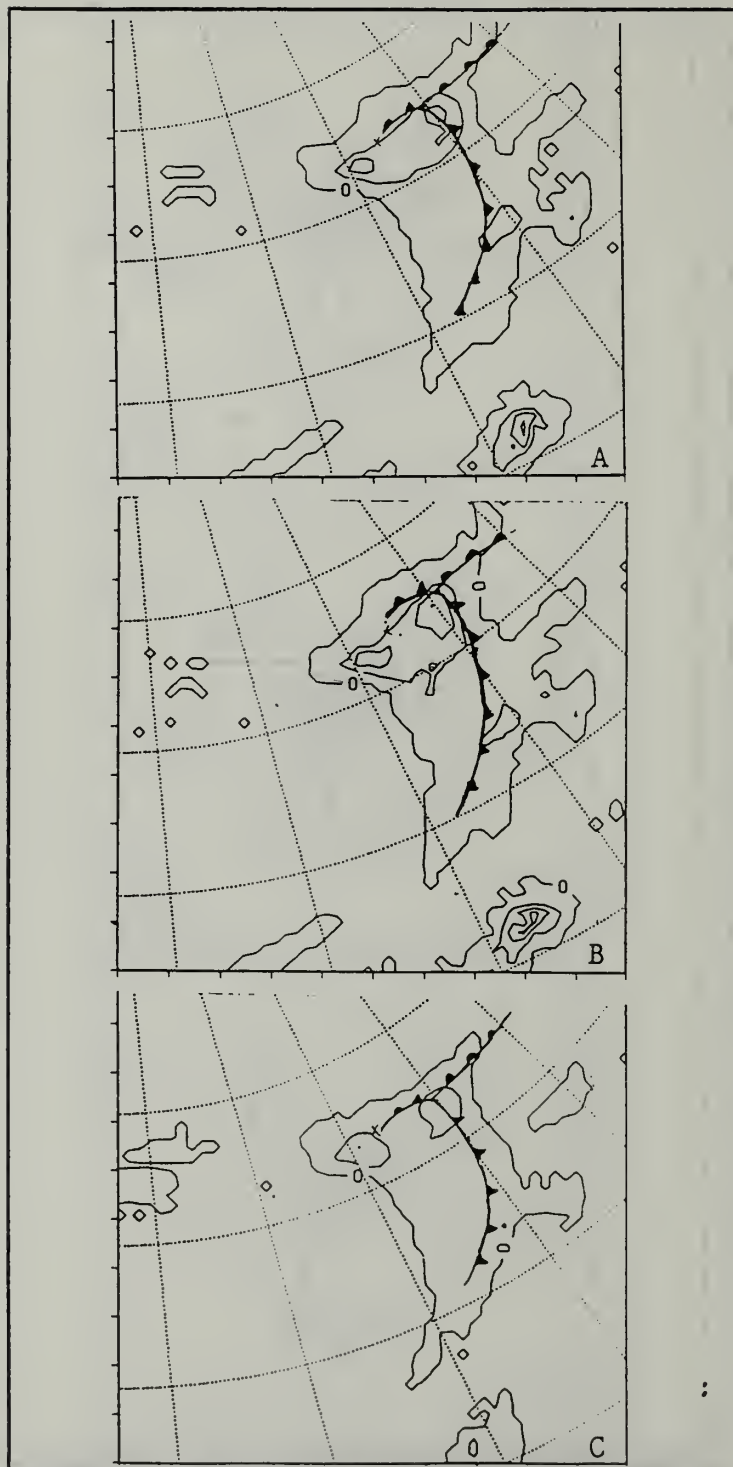
Figure 28. As in Fig. 26, except 48 h
forecast
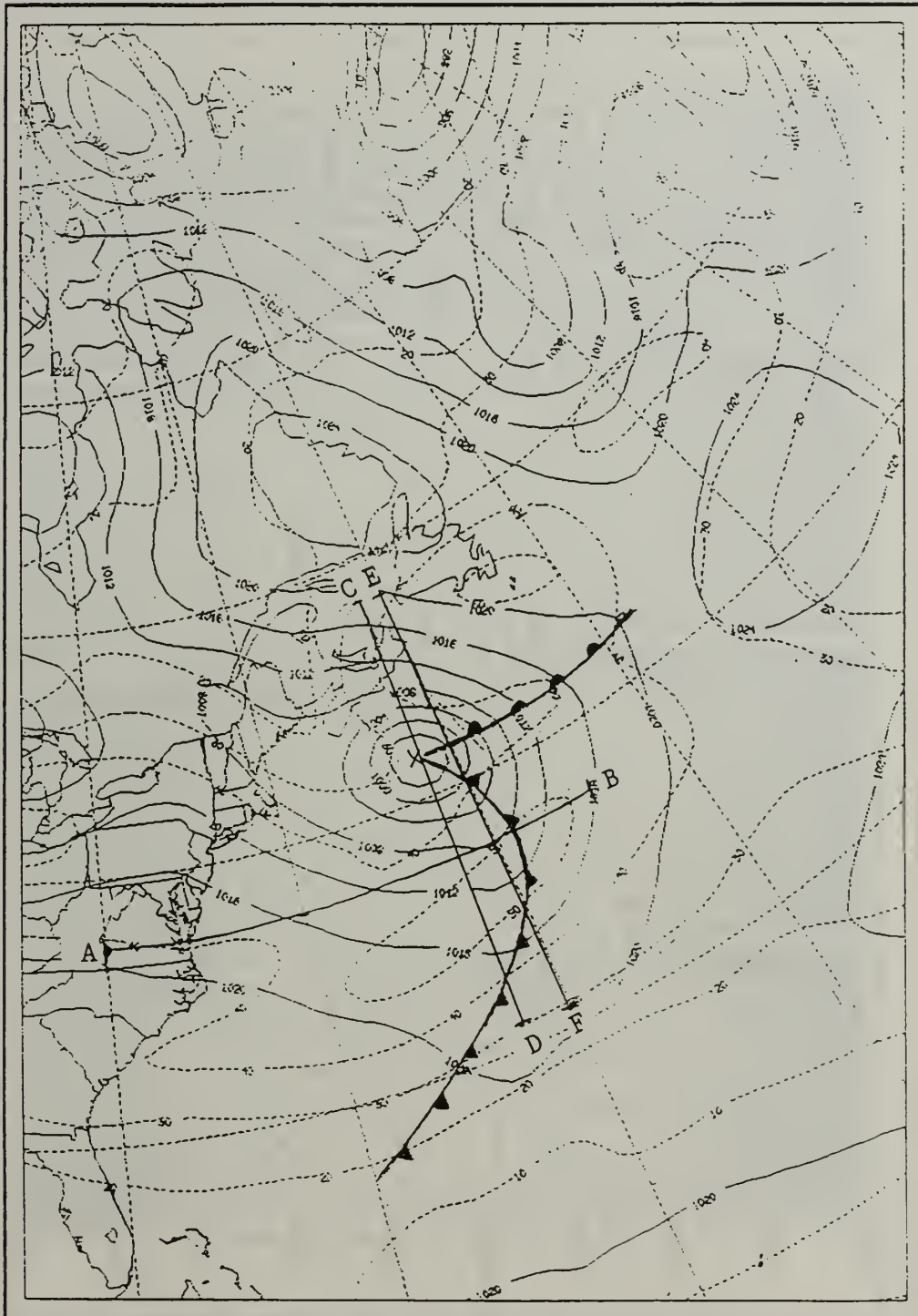
Figure 29. MSL pressure and 300 mb isotachs, 36 h OPNL
forecast: MSLP (solid) 4 mb increment; isotachs (dashed 10 m
s^{-1} increment. Cross sections AB, CD, and EF described in text.
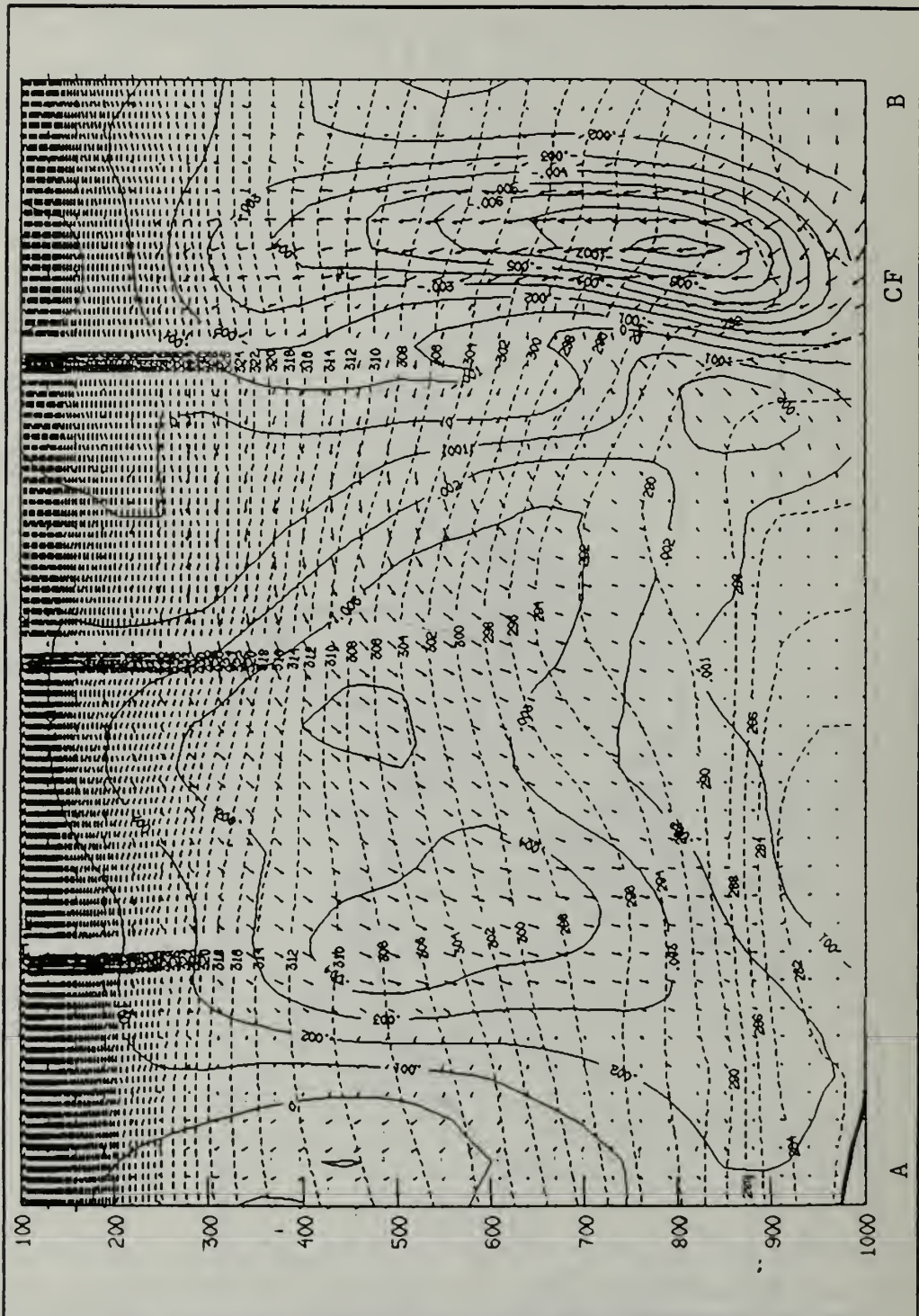
Figure 30. Potential Temperature and Omega, cross section AB:
36 h forecast for OPNL. Temperature (dashed) 2 K increment,
omega (solid) 1 μbar s^{-1} increment
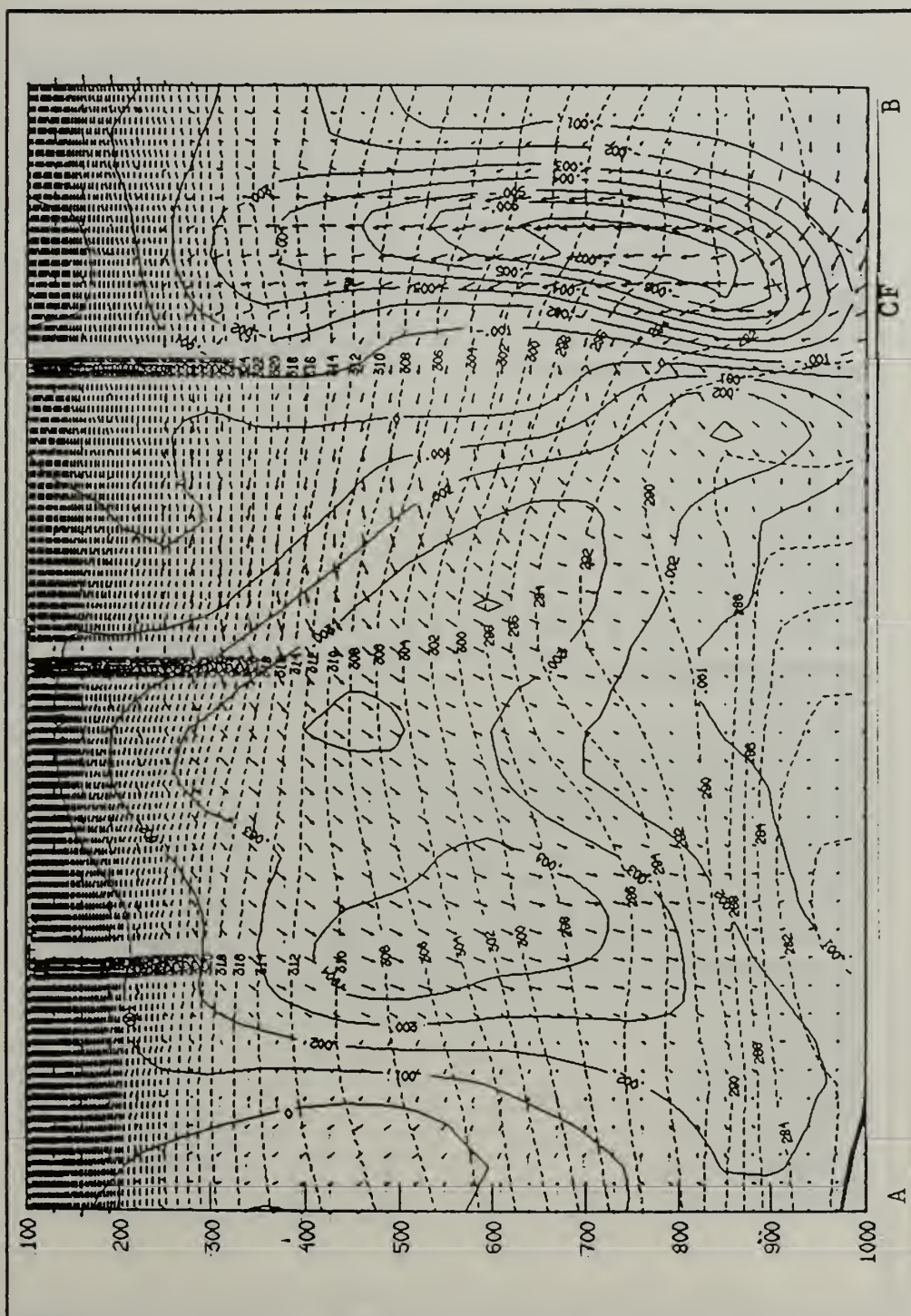
Figure 31. As in Fig. 30, except HSST

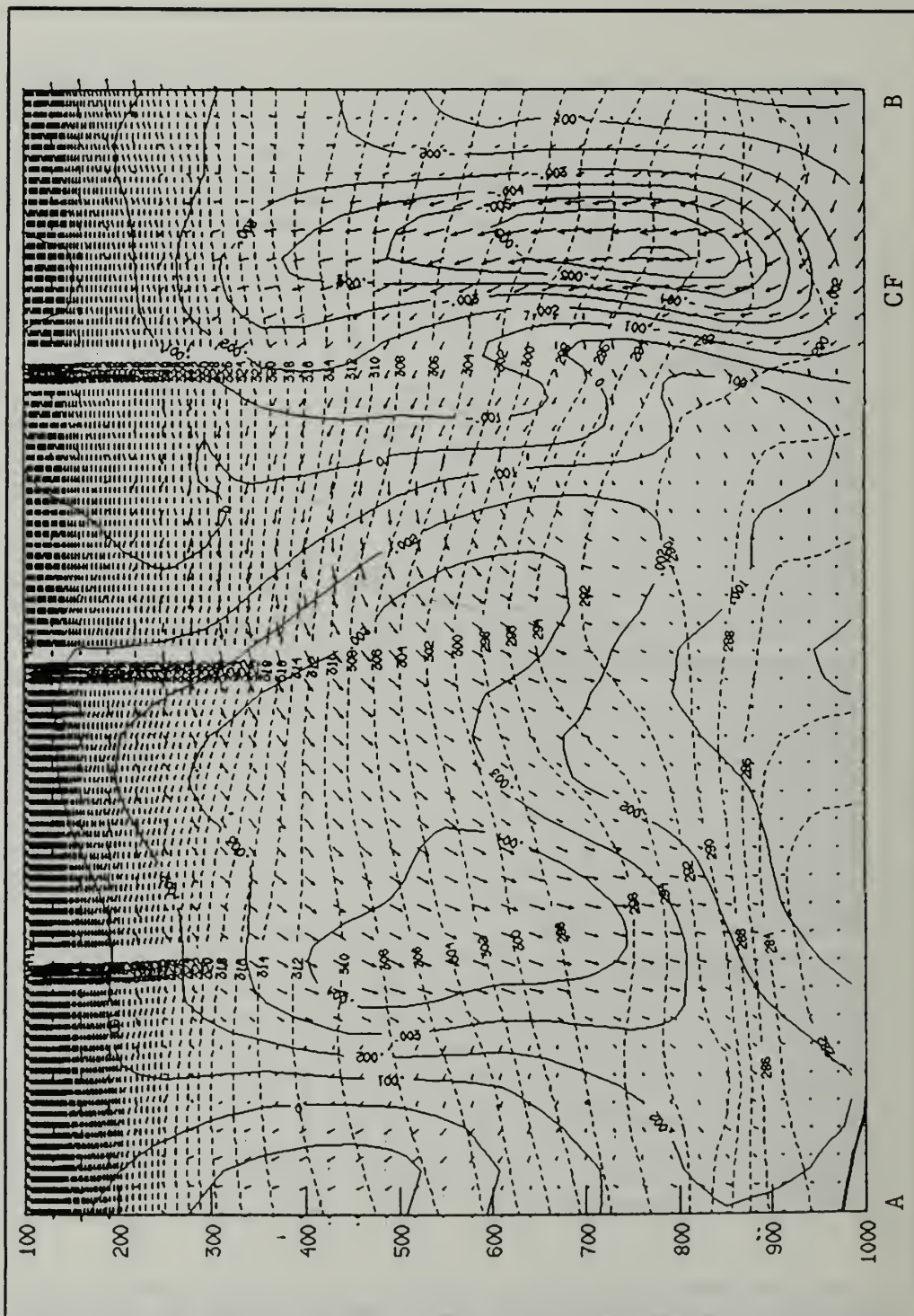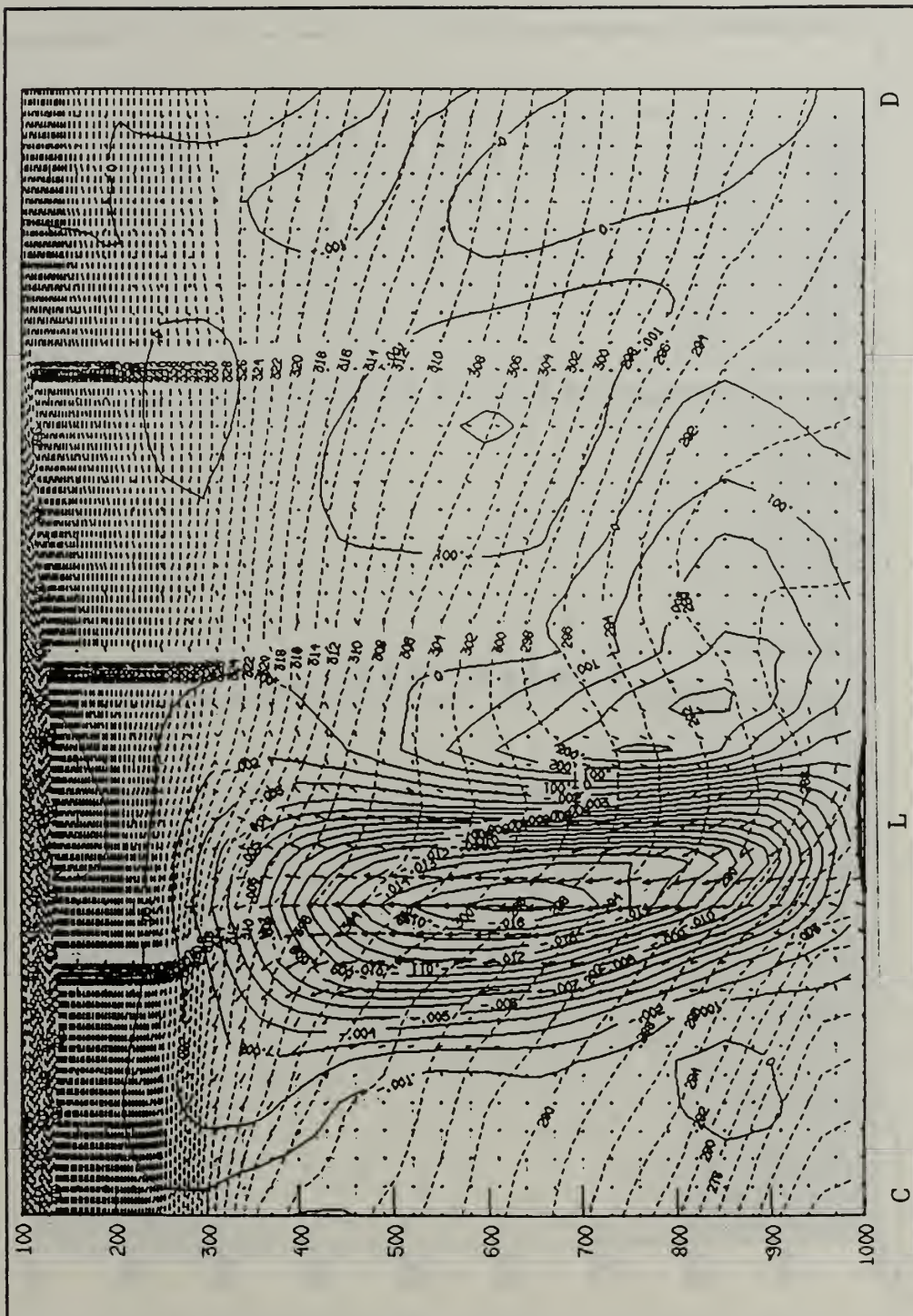Figure 32. As in Fig. 30, except NSF

64

Figure 33. As in Fig. 30, except cross section CD: 36 h
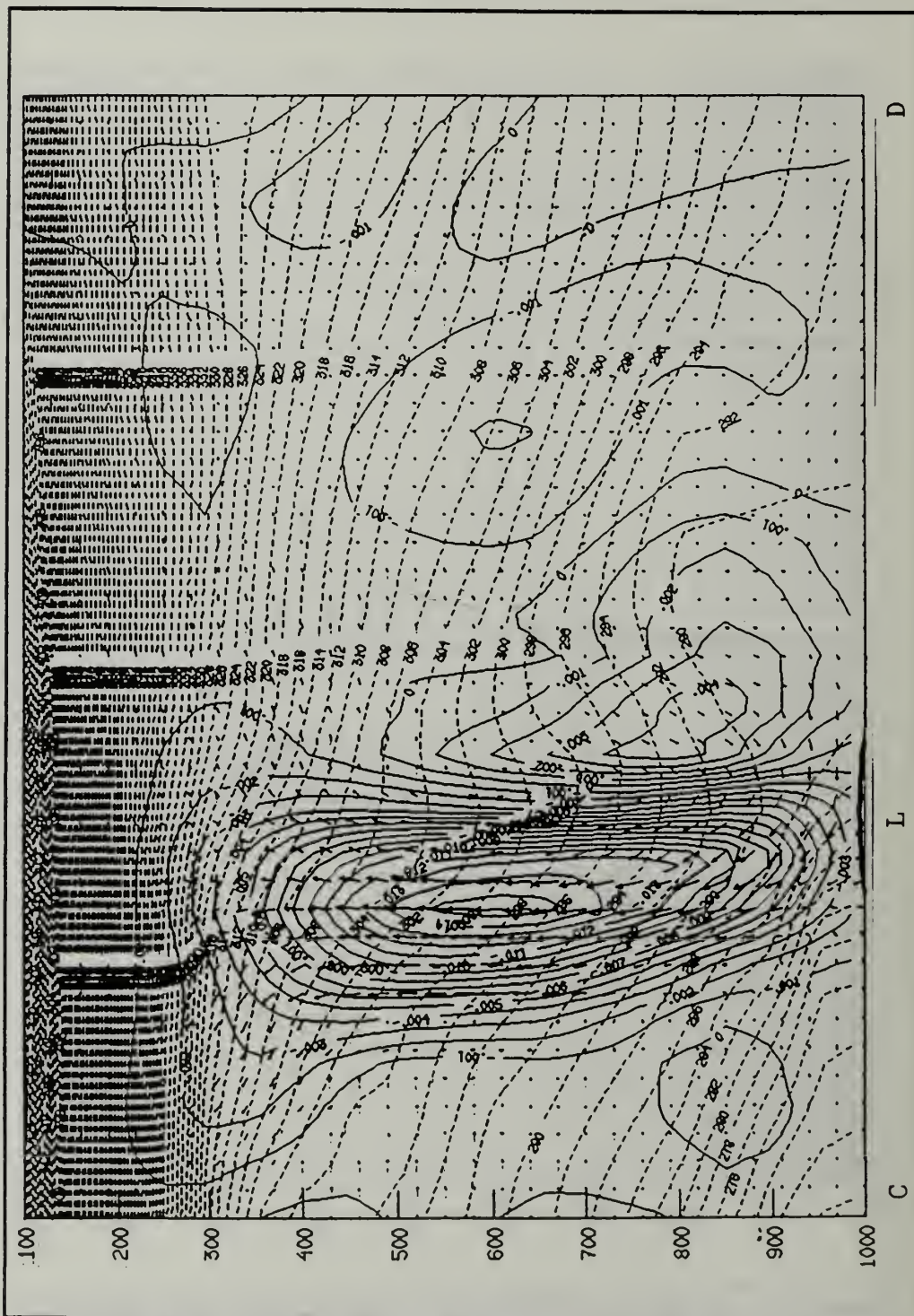forecast for OPNL

65

Figure 34. As in Fig. 33, except HSST

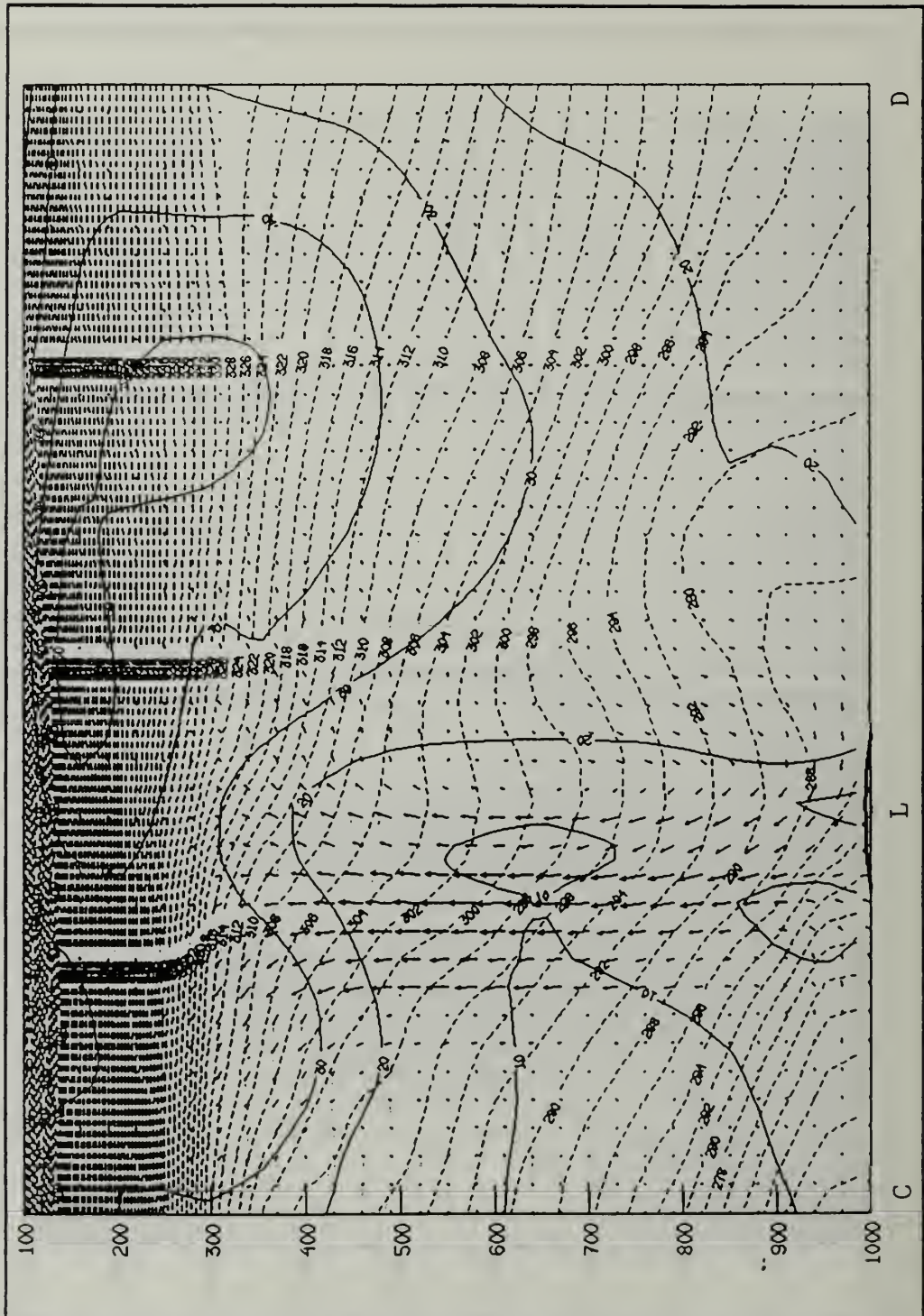Figure 35. As in Fig. 33, except NSF

67

Figure 36. Potential Temperature and Isotachs, cross section
CD: 36 h forecast for OPNL. Temperature (dashed) 2K increment,
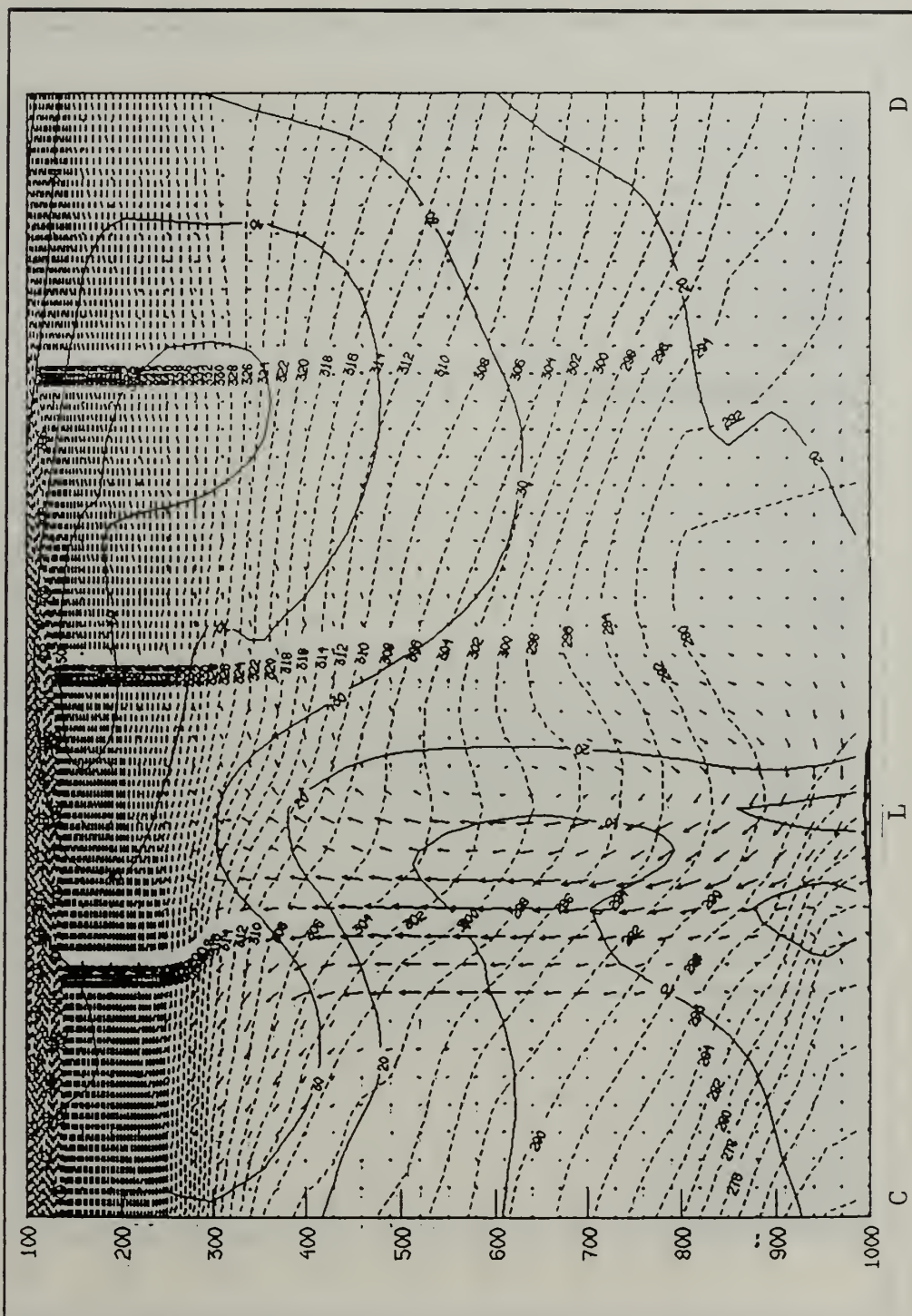isotachs (solid) 10 m s^{-1}
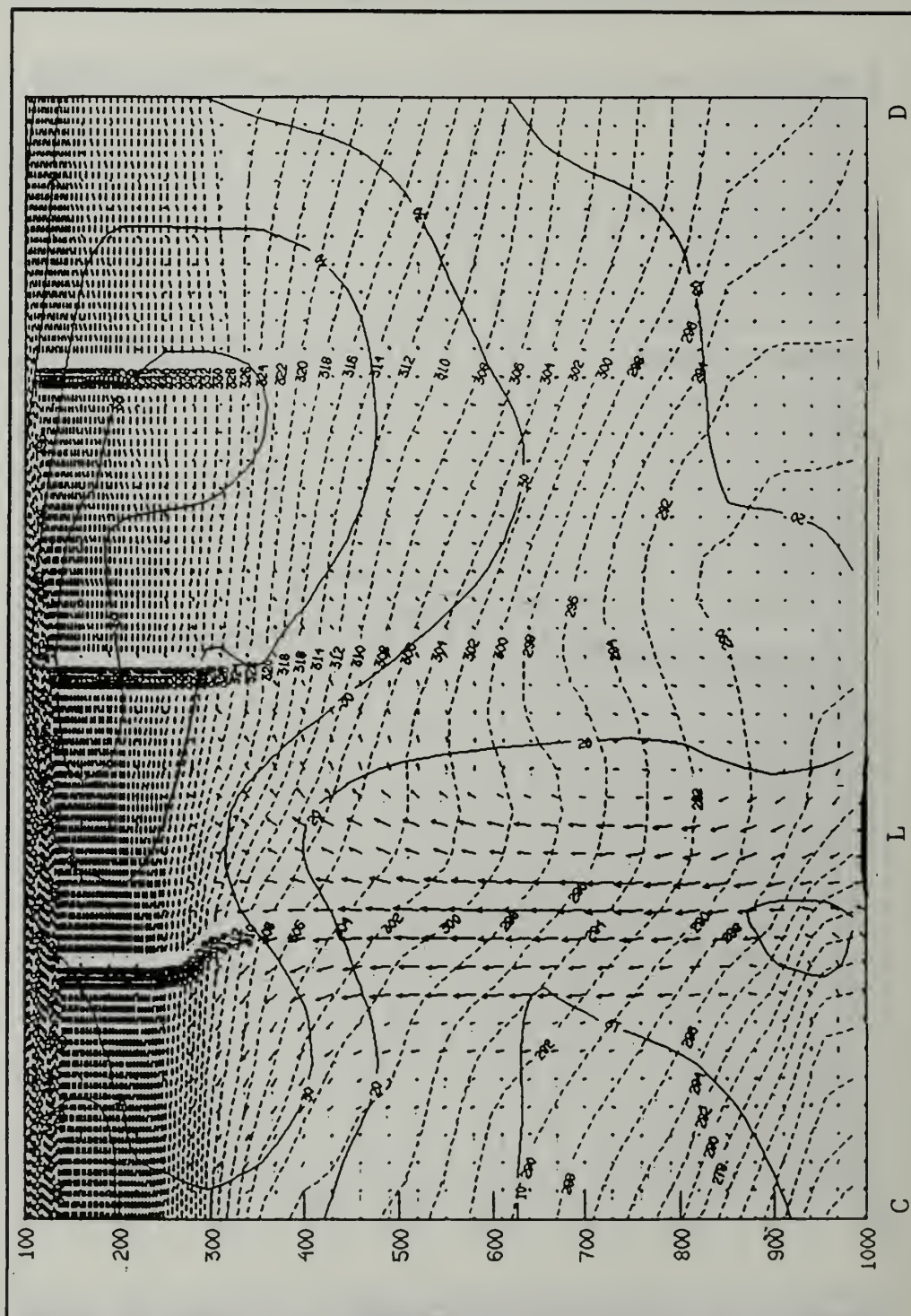
Figure 37. As in Fig. 36, except HSST

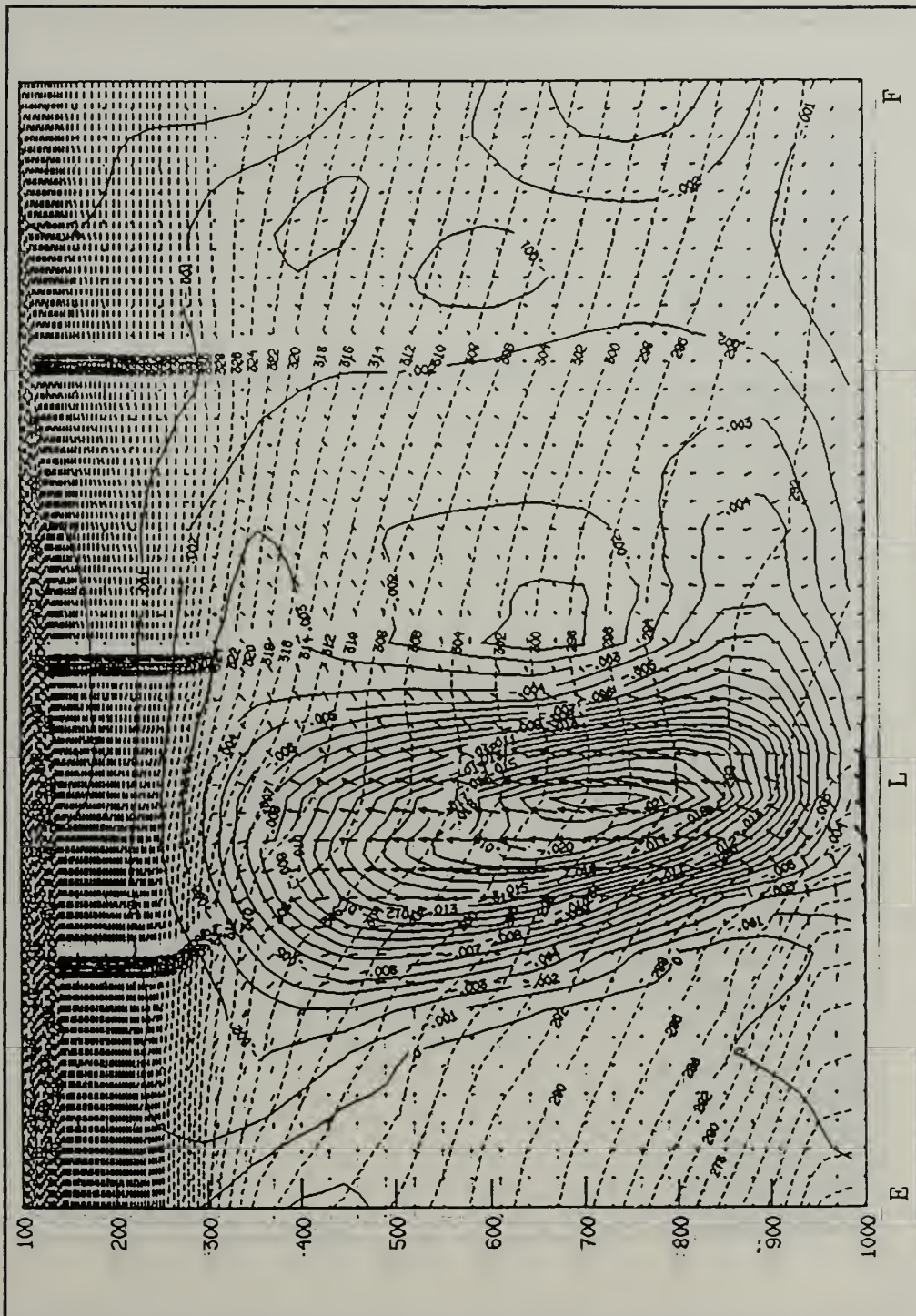69

Figure 38. As in Fig. 36, except NSF

Figure 39. As in Fig. 30, except cross section EF: 36 h
forecast for OPNL

71
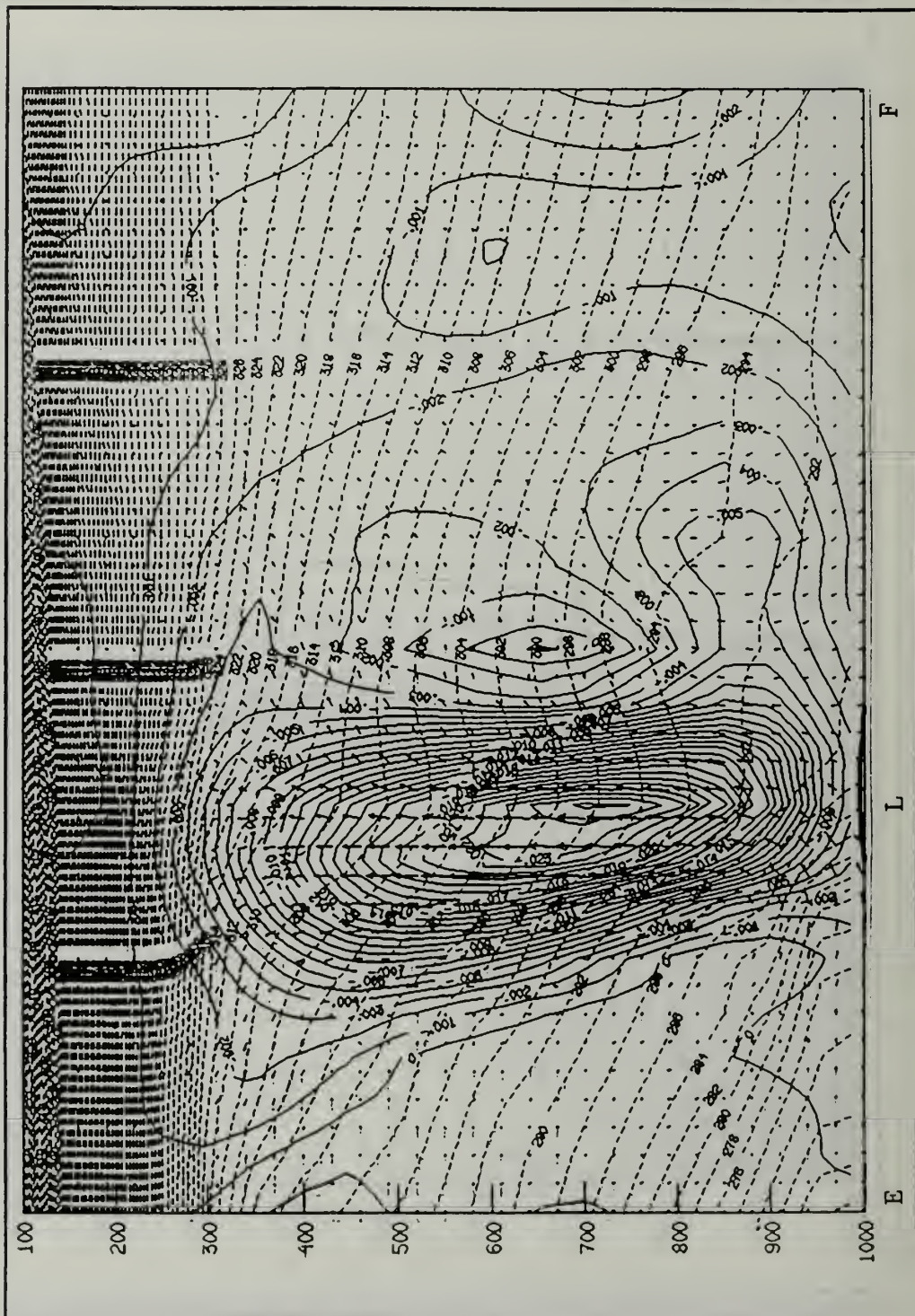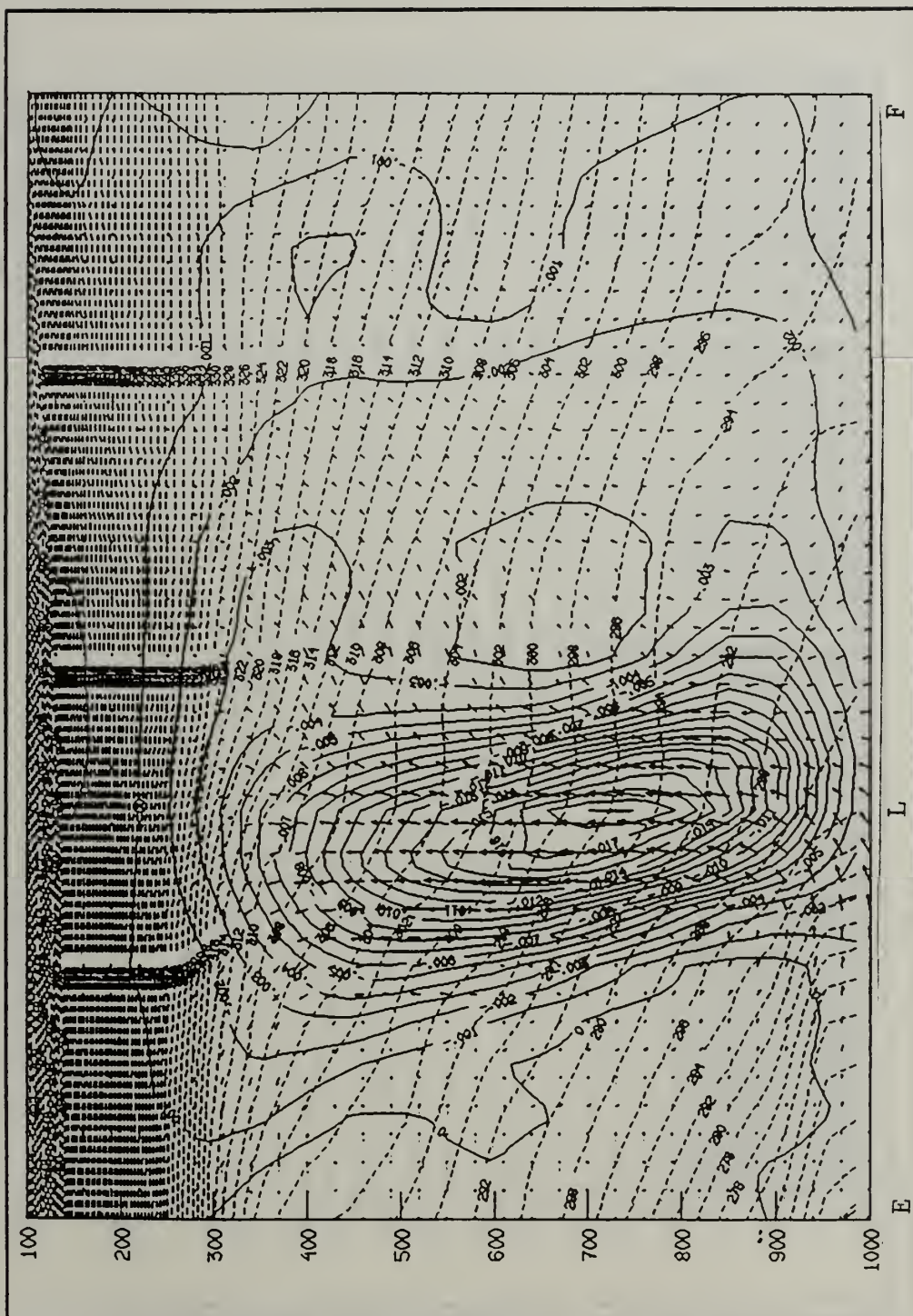
Figure 40. As in Fig. 39, except HSST
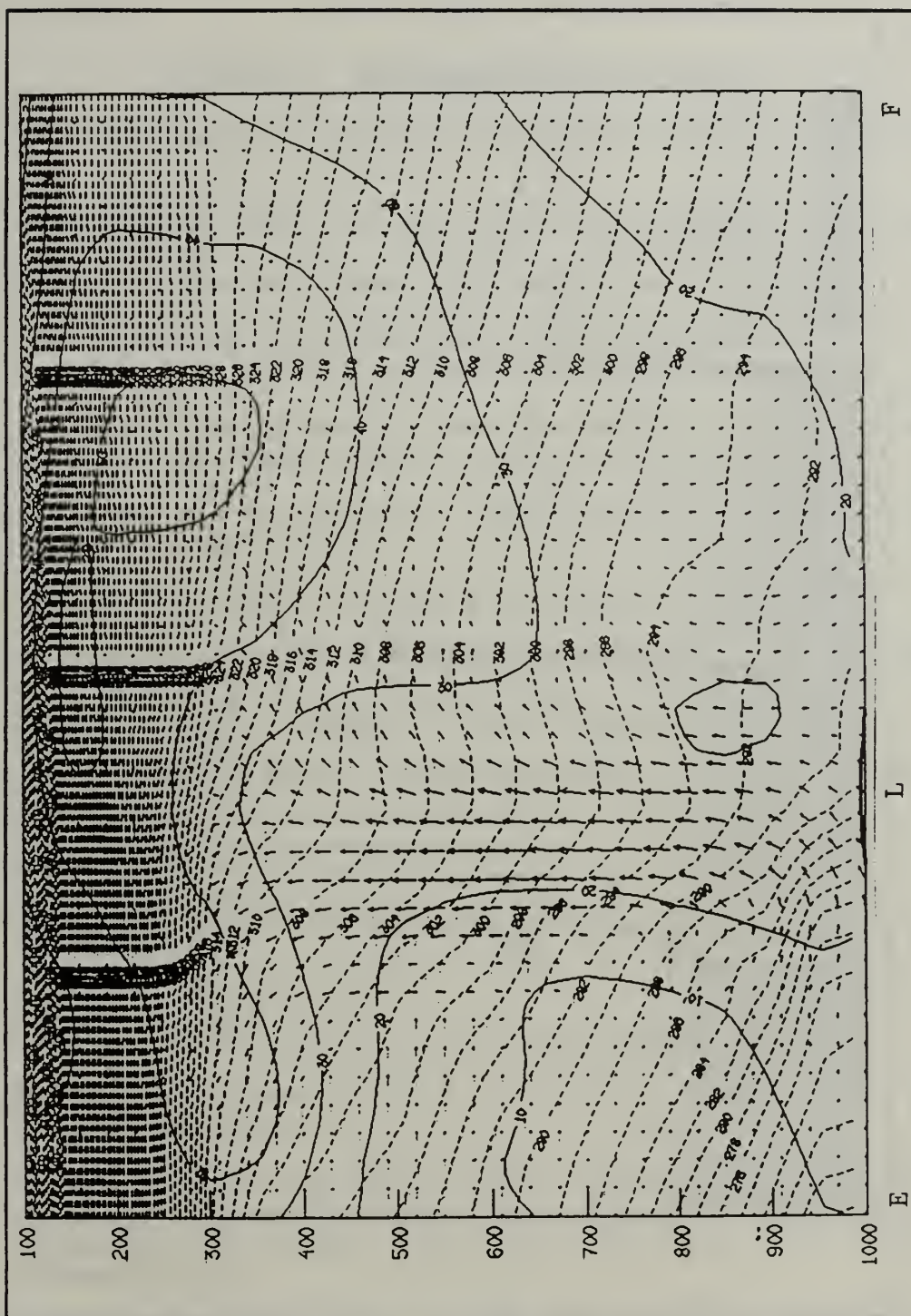
72

Figure 41. As in Fig. 39, except NSF

73

Figure 42. As in Fig. 36, except cross section EF: 36 h
forecast for OPNL

74

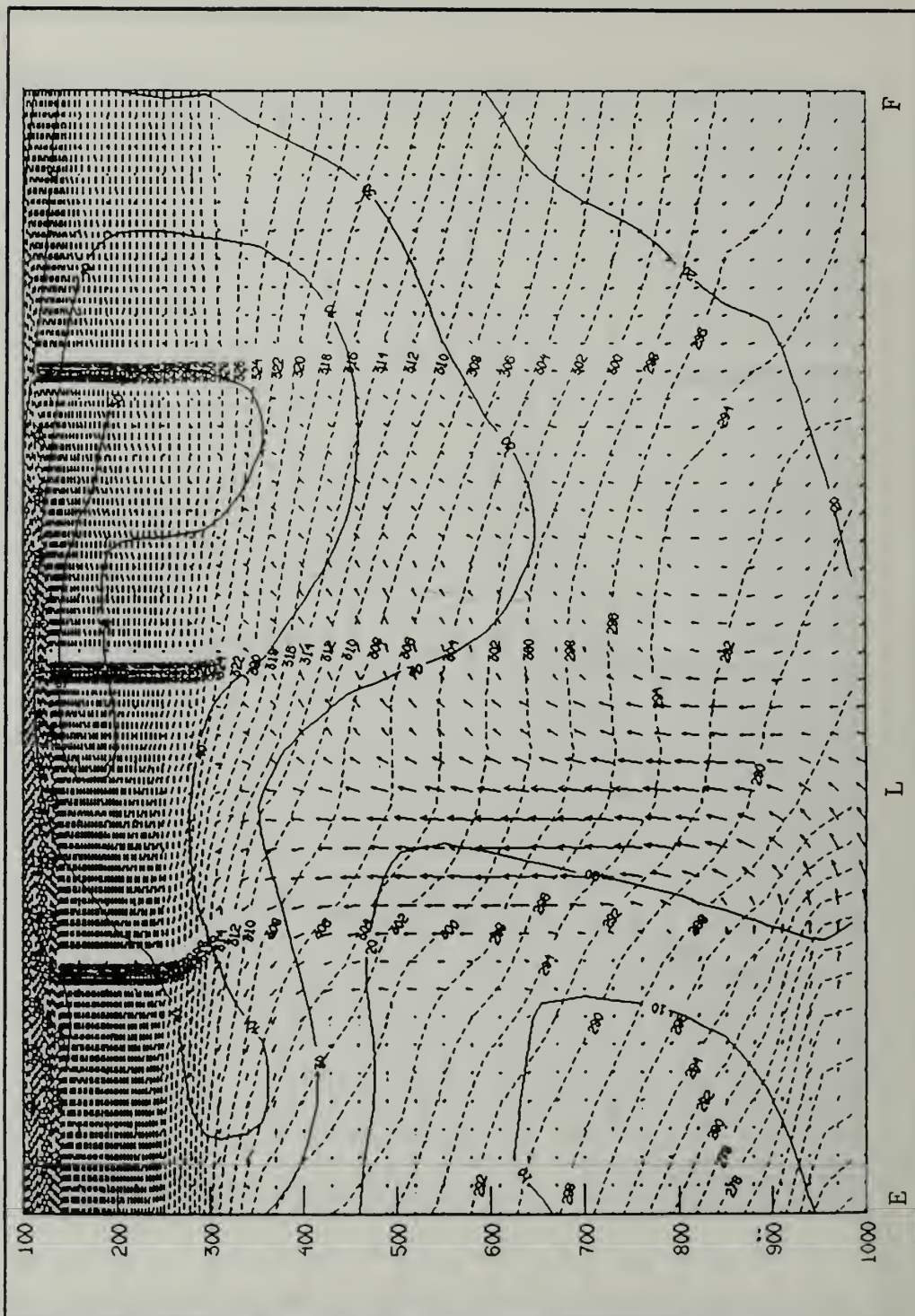Figure 43. As in Fig 42, except HSST

75

Figure 44. As in Fig. 42, except NSF

76

APPENDIX B: THE NESTED GRID MODEL (NGM)

The salient aspects of the NGM as described by Hoke et al. (1989) are:

* 3 nested grids: A-grid covering the northern hemisphere, 336 km mesh length at 45°N
  B-grid, covering North America and Arctic Circle,
    double resolution of A-grid with 168 km mesh length at 45°N
  C-grid, covering U.S., Canada and surrounding waters, double
    resolution of B-grid, 84 km mesh length at 45°N

* Two-way interactive boundary conditions between A and B and between B and C grids; symmetry imposed at equator for A-grid

* 16 layers, 13 in troposphere, with greatest resolution in the planetary boundary layer

* Variable depth planetary boundary layer (up to 6 layers)

* 6 h forecast first guess from Global Data Assimilation System (GDAS)

* Objective analysis: Regional Optimal Interpolation

* Temperton-Parrish implicit normal mode initialization of lowest two modes

* 48 h forecast period

* Differencing: Arakawa D-grid with Lax-Wendroff time differencing

* Inner grid time-step: 75 sec

* Stability dependent fluxes, bulk surface exchange

* Kuo cumulus parameterization, grid-scale precipitation, dry convective adjustment

* Post-processing: conversion of sigma to pressure surfaces, from 1000 to 100 mb in 50 mb increments; interpolation of horizontal wind components from momentum points to mass points resulting in an unstaggered grid

* Low-pass fourth-order Shapiro filter applied every 30 minutes during forecast period to control noise and for smoothing output

REFERENCES

Baker, F.W., 1991: *The effect of latent heat release on the ERICA IOP-5 cyclone.* M.S. Thesis, Naval Postgraduate School, 76 pp.

Ballentine, R.J., 1980: A numerical investigation of New England coastal frontogenesis. Mon. Wea. Rev., 108, 1479-1566.

Davis, C.A. and K.A. Emanuel, 1988: Observational evidence for the influence of surface heat fluxes on maritime cyclogenesis. Mon. Wea. Rev., 116, 2649-2659.

Feit, D.M., 1986: Compendium of marine meteorological and oceanographic products of the Ocean Products Center. NOAA Tech. Memo., NWS-NMC 68, 93 pp.

Greer, S.N., 1991: *Mesoscale surface analysis of the ERICA IOP-5 cyclone.* M.S. Thesis, Naval Postgraduate School, 65 pp.

Hadlock, R., and C.W. Kreitzberg, 1988: The Experiment on Rapidly Intensifying Cyclones over the Atlantic (ERICA) field study: Objectives and plans. *Bull. Amer. Meteor. Soc.*, 69, 1309-1320.

Hoke, J.E., N.A. Phillips, G.J. DiMego, and J.G. Sela, 1989: The Regional Analysis and Forecast System of the National Meteorological Center. Wea. Forecasting, 4, 323-334.

Kuo, Y.-H., and S. Low-Nam, 1990: Prediction of nine explosive cyclones over the western Atlantic Ocean with a regional model. Mon. Wea. Rev., 118, 3-25.

Kuo, Y.-H., R.J. Reed, and S. Low-Nam, 1991: Effects of surface energy fluxes during the early development and rapid intensification stages of seven explosive cyclones in the western Atlantic. *Mon. Wea. Rev.*, **119**, 457-476.

Lapenta, W.M., D.J. Perkey, C.W. Kreitzberg, and F.R. Robertson (1992): The role of the sea-surface temperature distribution on explosive cyclogenesis during ERICA. *Proceedings of the 5th Conference on Mesoscale Processes*, 91-96.

Mailhot, J., and C. Chouinard, 1989: Numerical forecasts of explosive winter storms: Sensitivity experiments with a meso-α scale model. *Mon. Wea. Rev.*, **117**, 1311-1343.

Petersen, R.A., G.J. DiMego, J.E. Hoke, K.E. Mitchell and J.P. Gerrity, 1991: Changes to NMC's regional analysis and forecast system. *Wea. Forecasting*, **6**, 133-141.

Petterssen, S., D.L. Bradbury and K. Pedersen, 1962: The Norwegian cyclone models in relation to heat and cold sources. *Geofys. Publ.*, **24**, 243-280.

Rao, D.B., 1989: A review of the program of the Ocean Products Center. *Wea. Forecasting*, **4**, 427-443.

Reed, R.J., and A.J. Simmons, 1991: Numerical simulation of an explosively deepening cyclone over the North Atlantic that was unaffected by concurrent surface energy fluxes. *Wea. Forecasting*, **6**, 117-122.

Roebber, P.J., 1984: Statistical analysis and updated climatology of explosive cyclones. *Mon. Wea Rev.*, **112**, 1577-1589.

Sanders, F., and J.R. Gyakum, 1980: Synoptic-dynamic climatology of the
    "bomb". *Mon. Wea. Rev.*, **108**, 1589-1606.

Uccellini, L.W., 1990: Processes contributing to the rapid development
    of extratropical cyclones, in *Extratropical Cyclones: The Erik
    Palmen Memorial Volume*, eds. C. Newton and E.O. Holopainen, Amer.
    Metero. Soc. Boston. 81-105.

---- and P.J. Kocin, 1987: The interaction of jet streak circulation
    during heavy snow events along the east coast of the United States.
    Wea. Forecasting, 2, 289-308.

Warner, T.T., M.N. Lakhtakia, J.D. Doyle, and R.A. Pearson, 1990: Marine
    atmospheric boundary layer circulations forced by Gulf Stream sea
    surface temperature gradients. *Mon. Wea. Rev.*, **118**, 309-323.

Wash, C.H., J.E. Peak, W.E. Calland, and W.A. Cook, 1988: Diagnostic
    study of explosive cyclogenesis during FGGE. *Mon. Wea. Rev.*, **116**,
    431-451.

INITIAL DISTRIBUTION LIST

		No. Copies
1.	Defense Technical Information Center Cameron Station Alexandria, VA 22304-6145	2
2.	Library, Code 52 Naval Postgraduate School Monterey, CA 93943-5002	2
3.	Chairman (Code MR/Hy) Department of Meteorology Naval Postgraduate School Monterey, CA 93943-5000	1
4.	Chairman (Code OC/Co) Department of Oceanography Naval Postgraduate School Monterey, CA 93943-5000	1
5.	Professor Patricia M. Pauley (Code MR/Pa) Department of Meteorology Naval Postgraduate School Monterey, CA 93943-5000	2
6.	Professor Wendell A. Nuss (Code MR/Nu) Department of Meteorology Naval Postgraduate School Monterey, CA 93943-5000	1
7.	LT Marcia DeCaria Naval Oceanography Command Detachment, Mayport Naval Station Mayport, FL 32228-0043	1
8.	Commander Naval Oceanographic Command Stennis Space Center MS 39529-5000	1
9.	Commanding Officer Fleet Numerical Oceanography Center Monterey, CA 93943-5005	1

10. Commanding Officer
    Naval Research Laboratory   1
    Stennis Space Center
    MS 39529-5004

11. Superintendent
    Naval Research Laboratory   1
    NPS Annex, Code 7500
    Monterey, CA 93943-5006

12. Chief of Naval Research
    800 North Quincy Street   1
    Arlington, VA 22217

894-215